Application of a Network Solution to Complex Fenestration Systems

by

Christine Rogalsky

A thesis
presented to the University of Waterloo
in fulfillment of the
thesis requirement for the degree of
Master of Applied Science
in
Mechanical Engineering

Waterloo, Ontario, Canada, 2011

I hereby declare that I am the sole author of this thesis. This is a true copy of the thesis, including any required final revisions, as accepted by my examiners.

I understand that my thesis may be made electronically available to the public.

Abstract

In the fight to reduce carbon emissions, it is easy to see the necessity of reducing energy consumption. Buildings consume a large amount of energy, and have significant potential for energy savings. One tool for realising these potential savings is building simulation. To be able to use building simulation, accurate models for windows are needed. The models include individual layer models, to determine the solar and longwave radiative behaviours, as well as whole-system models to determine heat flows through the various layers of fenestration systems.

This thesis looks at both kinds of models for incorporating windows into building simulations. A new network whole-system model is implemented, and integrated into the California Simulation Engine building simulation software. This model is also used as the calculation engine for a stand-alone rating tool. Additionally, a measurement technique used to measure off-normal solar properties of drapery materials, as part of developing shading layer models, is investigated using a Monte Carlo simulation.

The network model uses a very general resistance network, allowing heat transfer between any two layers in a complex fenestration system (CFS), whether they are adjacent or not, between any layer and the indoor or outdoor side, or between the indoor and outdoor sides, although this last case is unlikely. Convective and radiative heat transfer are treated using the same format, resulting in increased stability. This general resistance network is used to calculate indices of merit for the CFS using numerical experiments. This approach requires fewer iterations to solve than previous solution methods, and is more flexible.

The off-normal measurement technique which was investigated used a sample holder inserted into an integrating sphere. This is a non-standard way of using an integrating sphere, and early analyses did not provide conclusive information as to the effect of the sample holder. A Monte Carlo analysis confirmed the amount of beam attenuation as being 20% for the sample holder used in the experiments. Also confirmed was the effectiveness of dual-beam integrating spheres in correcting for the presence of a sample holder.

The stand-alone rating tool which uses the general network framework, incorporates an easy-to-use visual interface. This tool models multiple types of shading layers with no restrictions on how they are combined. Users can easily change any one layer to see the effects of different arrangements. Users may specify any combination of indoor and outdoor ambient and mean radiant temperatures, insolation, and beam/diffuse split.

Acknowledgements

I would like to acknowledge the assistance of my supervisor, Prof. J.L. Wright, who, in addition to providing me with this project, has been an invaluable resource for building modelling, and contacts in the field. This would not have been possible without his strong support.

I would also like to thank Prof. M. Collins and Prof. K. Daun for their assistance with the integrating sphere work included in this thesis, and for general support during my degree work.

Financial support from the Natural Sciences and Engineering Research Council of Canada (NSERC), University of Waterloo Presidents Scholarship and Faculty of Engineering Graduate Scholarships are also gratefully acknowledged.

Contents

List of Tables

List of Figures

Nomenclature

Greek Symbols

θ	An angle
ρ	Reflectivity (dimensionless)
τ	Transmissivity (dimensionless)
Φ	Flux ($\frac{W}{m^2}$)

Symbols

A	Area (m^2) or a specific area
C_x	Cross coupling coefficient ($\frac{W}{m^2K}$)
F	A view factor (dimensionless)
f	The port fraction
f_r	Weighting factor for determining effective ambient temperatures (dimensionless)
h	Heat transfer coefficient ($\frac{W}{m^2K}$)
I	Incident flux ($\frac{W}{m^2}$)
L	Radiance of a surface ($\frac{W}{m^2sr}$)
N	Inward-flowing-fraction (dimensionless)
n	Number, either of photon bundles or of layers in a complex fenestration system (dimensionless)

q Heat flow ($\frac{W}{m^2}$)

R Response of an integrating sphere (dimensionless)

r Radius of a sphere

S A chord in a sphere

S Absorbed energy, W

$SHGC$ Solar Heat Gain Coefficient (dimensionless)

T Temperature ($^\circ C$ or K)

U Overall coefficient of heat transfer ($\frac{W}{m^2 K}$)

Subscripts and Superscripts

a Air, ambient - relating to convection

ae Ambient effective, referring to a weighted average of air and radiant temperatures

c Convective

c Cross sectional

cg Center-of-glass

exp Experimental

in Indoor or incoming

m Mean radiant - relating to radiation

$meas$ Measurement beam

out Outdoor side

r Radiative

ref Reference beam

rep As reported

s	Surface
sol	Solar
t	Rotal
$tube$	relating to the sample holder tube

Chapter 1

Introduction

Greenhouse gas emissions have become a pressing global problem. Although alternative energy sources are being investigated, the most effective way to reduce greenhouse gas emissions is simply to lower energy use. One area for reducing energy usage with considerable savings potential which is often overlooked is buildings. Buildings account for over 31% of total energy used in Canada (The Report of the National Advisory Panel on Sustainable Energy Science and Technology, 2006). There is a lot of room for reducing building energy usage, as many buildings do not incorporate even cost-effective energy-saving measures. Changes to building energy use, therefore, are a very practical way to make substantial reductions to overall energy usage.

One important tool in designing more energy-efficient buildings is to use building simulations, which provide a faster and simpler way to determine the heating and cooling loads in a building. Conventional practice for selecting HVAC equipment is to oversize the equipment. The design conditions for selecting equipment are conservative, and so tend to overestimate the load. In addition, the design condition is a worst-case scenario, and most of the time less capacity is required (McQuiston, P.E. and Spitler, P.E., 1992). In using a simulation program to select heating and cooling equipment, the peak loads and the required capacity of the equipment can be predicted more accurately. This results in operational energy savings, as higher efficiency can be realised by equipment that operates at closer to the rated load.

In addition to more accurately predicting the transient responses of buildings, building simulations are an easy way to look at more complicated factors, like interactions between

multiple features in a building, such as improved insulation giving a higher-efficiency furnace more opportunity to save energy. These interactions are often too complex to be practical to examine if a building simulation isn't used. It can also be a useful way to judge trade-offs. For example, adding windows can allow for a decrease in electric lighting, but will also result in an increased cooling load, while potentially lowering the total heating energy consumption due to solar gain through the window. At the same time, the peak heating load will increase, as windows have low thermal resistance, and peak heating load occurs at night, when there are no solar gains.

The primary goal of building simulation is determining the amount of energy gained or lost by the building, with emphasis on the building envelope. Environmental conditions, such as temperature differences between the inside of the building – the conditioned space – and the outside, as well as energy gain due to solar radiation are significant driving factors in building energy balances. A large part of the heating and cooling loads are defined by these energy flows. Modelling heat flow through windows is more complicated than modelling a wall without windows, but windows are necessary features for many reasons.

The standard measure of a wall's thermal performance is the U-value, which is a measure of the amount of heat that will be transmitted through the wall due to a temperature difference, the reciprical of thermal resistance. For more detailed modelling, this heat gain can be split into its heat transfer components, as radiative heat gain has a different effect on building load than does convective heat gain. The U-value applies to windows also, but in addition to heat transfer through windows, a window has the potential for solar gain due to direct transmission of radiation. This gives rise to a second index of merit for windows, known as the solar heat gain coefficient, or SHGC. SHGC is the portion of the insolation which is transmitted as heat to the conditioned space. In general SHGC$= \tau + \sum_0^n N_i A_i$ where τ is the fraction of solar radiation directly transmitted through the window, A_i is the fraction of solar energy absorbed in layer i and N_i is the inward flowing fraction from layer i, or the portion of the absorbed energy which flows to the inside rather than back out. A more complete development is available in the literature (e.g. Wright and McGowan, 1999). This heat gain can be a significant problem, as energy-efficient buildings are generally well-insulated, resulting in heat gain being retained. It is possible to design windows that will result in lower heat gain, but this only increases the need for accurate simulations of windows.

As more accuracy is required, modelling windows becomes more complicated. As an example, shading devices are popular as a way to reduce solar gains. Shading devices are also common to reduce glare, provide privacy and to cut back on excess light. The addition of these devices creates what is known as a complex fenestation system or CFS, and requires more elaborate calculations to be able to predict the energy flow through the window. Even the addition of an insect screen can make a significant difference both in the amount of energy that enters a conditioned space, and the relationship between convective and radiative heat gain (Brunger et al., 1999). Shading devices cannot be ignored if accuracy is required, so modelling a complex fenstration system is itself a complex problem.

1.1 Previous Work

1.1.1 Calculating solar gain

A very detailed model for determining solar gain of complex fenestration systems was developed by Klems (1994a,b). Prior to this model, solar gain was primarily determined by measuring the solar gain of a specific system in a calorimeter. As more layers became available, the possible number of systems which would need to be classified began to grow to unmanageable numbers. Klems' model allowed for solar gain to be calculated from any combination of characterised layers, rather than requiring that the specific combination be characterized. For this model, a layer does not need to be a glazing layer, but can also be a shading layer such as a venetian blind or an insect screen. To characterise a layer, directional reflection and transmission measurements of the layer are made. The directions in which the radiation is reflected and transmitted, as well as the fraction of radiation in each direction are recorded. These measurements are repeated for all directions of incoming radiation. For spatially inhomogeneous layers, such as venetian blinds, the transmittance and reflectance are spatially averaged over the entire layer. This averaging is applicable unless the system has two layers with spatial inhomogeneities in the same dimension in the same scale.

To take these measurements, Klems (1994a) defines 140 directions to discretize the directions from which radiation could come, or directions through which radiation could be transmitted or reflected. This allows the the transmittance and reflectance characteristics of the layer to be described with a matrix, where each row describes an incident direction, and each column describes an outgoing direction. This matrix allows the radiance transmitted through one layer to be turned into incident radiation on the next layer. To take inter-reflections into consideration, Klems (1994b) uses an infinite series to sum the reflections and determine the total radiation incident on a surface. The absorbed radiation at each layer is found by applying an energy balance to each layer. This is extremely computationally intensive, in addition to needing large amounts of measured data, and as such is not well suited for use in building simulations.

To simplify calculations, instead of describing the incident radiation in terms of how much is coming from each direction, it can be described as being a combination of beam radiation from only one direction, and purely diffuse radiation, with the light coming from

every direction evenly (e.g. Wright and Kotey, 2006; Laouadi and Parekh, 2007; Klems et al., 1997). The reflection and transmission of the diffuse radiation is determined by integrating the transmissivity over incoming radiation from every direction. The reflection and transmission of the beam radiation are determined based on the incidence angle of the beam radiation. To find a total transmittance of the glazing, the two transmittance values can be combined by weighting them by the amount of incident beam and diffuse radiation.

For a two-layer system, the radiation which is transmitted through the first layer is incident upon the second layer. Light which reflects from the second layer can be transmitted back through the first layer, increasing the reflectivity of the system as a whole. Additionally, beam radiation can be scattered by reflection from or transmission through a given layer, changing the diffuse-beam split of the light that is incident on the front of the second layer or reflected on the back of the first layer. All of these complicating factors result in multi-layer systems being significantly more complicated than systems which contain only one layer. Determining total reflectivity and transmissivity of a multi-layer system can either be done layer-by-layer, as described by Laouadi and Parekh (2007), or as a whole system calculation as described by Wright and Kotey (2006).

To calculate the total system characteristics layer-by-layer, the first two layers are combined, and the total system reflectivity and transmissivity is determined. To add layers beyond two, the calculation is repeated, treating layers 1 through n-1 as a single layer, using the system reflectivity and transmissivity that was calculated in the previous step in lieu of the layer reflectivity and transmissivity. Layer n is used as the second layer, and is combined with the effective layer just as two layers are combined. This process is continued until all layers have been added (Laouadi and Parekh, 2007).

To calculate the transmissivity and reflectivity using a whole-system calculation, the diffuse and beam radiation are addressed in two different calculations. These calculations are linked by the scattering of beam radiation, which changes a portion of the beam flux to diffuse flux. The flux between each pair of layers is unknown, and is split into an inward travelling flux and an outward travelling flux. Each flux can be described as a combination of the unknown flux coming through the layer on one side of the gap, and the equally unknown flux reflecting off of that same layer, which is a known percentage of the flux in the other direction. If diffuse flux is being considered, both the transmission and reflection of diffuse flux, and the diffuse transmission and reflection of beam flux are used. The beam and diffuse fluxes can be found simultaneously. Alternatively, the beam fluxes can

be found first and the scattered beam radiation treated as sources of diffuse radiation, and the diffuse radiation fluxes solved for. This method is sufficiently general to allow flux from the inside of the window, such as would come from other windows or indoor lighting (Wright and Kotey, 2006). This method is similar to the method described by Edwards (1977), with the addition of a treatment for diffuse radiation, and beam-to-diffuse reflection and transmission.

These methods for determining solar transmission and reflection of complex fenestration systems all describe layers using a consistent set of solar-optical values. These are referred to as the effective layer properties. Any two layers with the same effective layer properties will have the same reflectivities and transmissivities. Additionally, substituting one of these layers for another in a complex fenestration system will not affect the overall properties of the system. Although the above descriptions are mostly in terms of glazing layers, if a shading layer can be described in the same manner as a glazing layer, it can be incorporated into the calculations in the same manner as a glazing layer.

1.1.2 Effect of Shading Layers on Heat Transfer

Instead of taking measurements at each point in the grid proposed by Klems (1994a), it is simpler and more practical to characterise a shading layer in such a way that the properties at different angles can be easily calculated. This is especially valuable for venetian blinds, as the layer properties vary not only with the angle of incidence, but with the slat angle. Fully characterising a venetian blind layer through measurement would require that the time-consuming process of characterising the layer be repeated for each slat angle.

Shading layer models have been around for a long time. Earlier models were limited compared to today's models, due to the lack of electronics when these models were being developed. Modern instrumentation allows for better measurements when characterizing layers. Additionally, the advances in computing power provide much high computational ability. This increased computational ability allows for more complex models, which can consider more factors and better represent the actual shading layers.

Venetian Blinds

Venetian blind models provide the beam and diffuse reflecting and transmitting characteristics of a layer of slat-type shades, using the slat solar properties, the slat width, thickness and spacing and the profile angle of the sun, as shown in Figure 1.1.

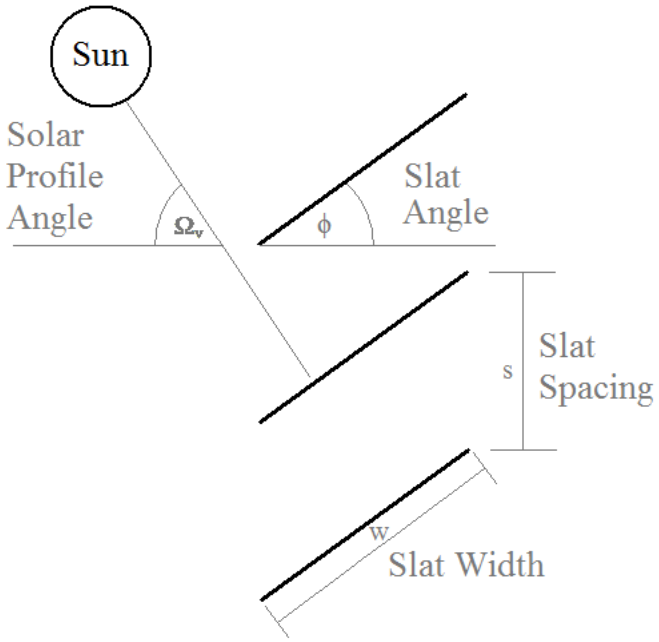

Figure 1.1: Venetian blind slats

The earliest attempt to develop a model of solar gain through venetian blinds was by Parmelee and Aubele (1952). This model was tested experimentally and was found to be accurate, although the measurements were limited by the ability to accurately measure the surface-optical properties of the slats used in the experiments (Parmelee et al., 1953). The model can handle slats which reflect either specularly or diffusely. More realistic surfaces can be modelled by separating the reflected radiation into these two components. Their paper presents curves for the transmittance and absorptance of slat assemblies of various geometries for both of these cases. Radiation striking the slats is assumed to be either reflected or absorbed, so the solar optical characteristics of the slats can be completely defined by the absorptance of the slats. Curves for the transmittance and

absorptance of diffuse radiation are not given, as those are calculated using a weighted sum of the transmittance for radiation coming from different directions. The paper defines an "Opening Ratio" which gives the portion of the direct solar radiation which passes through the slats without being reflected. A set of curves gives the opening ratio for various w/s ratios and Ω_v's. Although the curves were given for lookups, rather than for a simulation, the equations used to generate the curves are included in appendices, and could be incorporated into a computer simulation. Slats were assumed to be flat, and a correction for slat thickness is used. The upper and lower sides of the slats must have the same reflectance.

To calculate transmittance and absorptance for slats with specular reflection, the beam radiation is assumed to either travel between the slats without reflecting, reflect away from the slat assembly, reflect between the slat and the one above or below it and into the room or out again, or be absorbed. Ray tracing was used to determine how many reflections the beam will undergo for a given combination of slat width to slat spacing ratio, slat angle and solar angle. (Parmelee and Aubele, 1952).

Pfrommer et al. (1996) used similar methods to develop a model which could accurately represent a slatted shade without requiring time-intensive calculations, for GLSIM-BLIND. Both beam and diffuse radiation are considered, and reflection from the slats is considered to be a combination of diffuse and specular reflection. Direct transmittance is calculated using w/s, ϕ and Ω_v. The portion of the beam which reflects specularly is traced for an infinite number of calculations, until it all either is absorbed, reflected away from the slat assembly, or transmitted through the slat assembly. Diffusely reflected beam radiation is tracked for two reflections only, as this was found to result in error of less than 5%.

Another venetian blind model is presented by Yahoda and Wright (2005) which determines effective layer properties for venetian blind layers. The model was developed by using an enclosure between two slats as representative of the entire blind. As with other models, the slats are assumed to have both specular and diffuse reflection characteristics. The beam-beam transmission considers both the directly transmitted beam radiation as well as beam radiation transmitted after one or more specular reflections. Beam-diffuse radiation considers not only the portions of the slats which are directly illuminated by beam radiation, but also those which are illuminated after one or more specular reflections. Diffuse transmission and reflection, both diffuse-diffuse and beam-diffuse, are determined through enclosure theory. There are 8 surfaces total, including two pseudo-surfaces at the indoor

and outdoor sides of the enclosure. Each slat is divided into up to 3 sections, the divisions of which are determined by the locations of where the incident beam and reflections strike the slats, as shown in Figure 1.2. Depending on ϕ and Ω_v, as many as 7 or as few as 4 of the surfaces will be used. Light which is incident on surface 8 from the inside of the enclosure is diffusely transmitted to the indoor side. Light which is incident on suface 1 from the inside of the enclosure is diffusely reflected back to the outdoor side.

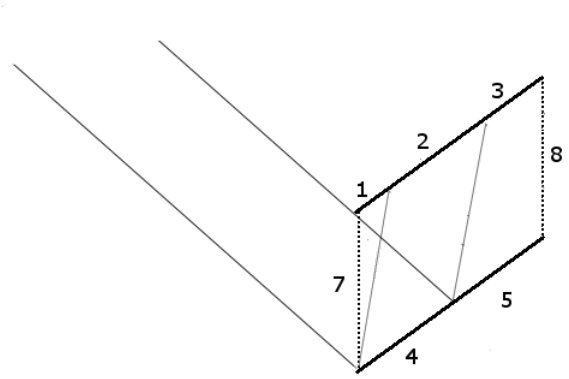

Figure 1.2: A venetian blind enclosure such as used by Yahoda and Wright (2005). The boundaries between surfaces are defined by where beam radiation and initial reflections strike the surfaces of the slats. Suface 6 is not present due to the relative solar and slat angles.

Kotey (2009) developed a model which allows for slats which transmit some radiation. This model is based on that of Yahoda and Wright (2005). The slats were assumed to be flat with negligible thickness, and to reflect and transmit diffusely. Beam-diffuse transmittance and reflectance are found using a six-surface enclosure shown in Figure 1.3. The radiosity of each surface is a function of the reflectivity and transmissivity of the slat, and of the radiation incident on that surface. Additionally, surface 4 has a source of diffuse radiation from the incident beam radiation. As in the previous model, the transmitted radiation is the radiation incident left-to-right on surface 2, and the reflected radiation is that which is incident right-to-left on surface 1.

If the entire slat surface is illuminated by the beam, then surfaces 5 and 6 do not exist, and a four-surface enclosure is used. Surfaces 3 and 4 have sources of diffuse radiation from the incident beam radiation which is transmitted through and reflected from the

slats respectively. Diffuse-diffuse properties are calculated using the four-surface model with a diffuse source on surface 1.

Since slats are normally curved, the model also includes a correction for slat curvature. This corrects for the fact that at some slat angles the curvature of the slat results in less transmission than if the slat was flat. This correction was developed using a geometric analysis of how the curvature of the slats would affect transmission at various ϕ and Ω_v combinations. When this is applied the modelled transmission is a much closer match to the measured transmission (Kotey, 2009).

Other Shading Layers

Although tests to determine the properties of specific shading layers have been conducted, the large variety of shading devices on the market makes models necessary due to the large amount of time required to test a shading layer. Due to this demand for models for shading

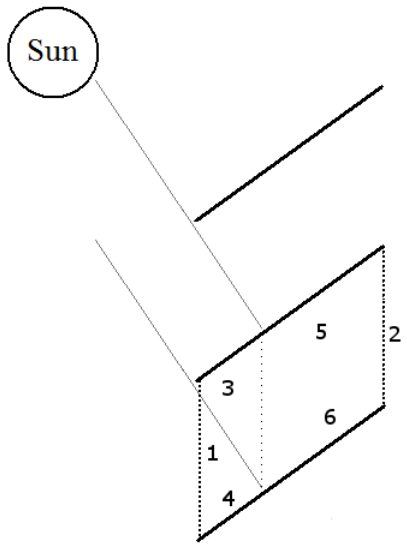

Figure 1.3: The 6 surfaces of a venetian blind slat enclosure. The boundary between surfaces 3 and 5 and between surfaces 4 and 6 is based on where the beam radiation strikes the slat.

layers, Kotey, Wright, and Collins (2009a,b,c,d) developed models for the behaviour of other shading layers: insect screens, roller blinds and pleated drapes. These models can be found in detail in Kotey (2009). This was aided by the development of a novel technique to measure off-normal solar properties of layer materials.

The models developed by Kotey (2009) give the transmittance and reflectance properties of the layer for beam and diffuse radiation, from the angle of incidence of the beam radiation and the normal incidence properties of the layer. By testing different samples of each type of material at various angles, models were found to describe how the reflectance and transmittance of the materials changed with incidence angle. These models can be used to determine the behaviour of roller blinds and insect screens in complex fenestration systems. To model pleated drapes, these equations are used as a basis to describe the behaviour of the drape fabric, which is then used in a model of the pleated drape as a whole. The beam-beam transmittance is directly related to the openness of the material – the open portion of the material through which radiation can pass without interacting with the material.

The model for a pleated drape gives the beam and diffuse transmittance and diffuse reflectance for a pleated drape layer. This model uses the fabric model, the folding ratio, and Ω_v and Ω_h of the incident radiation. The folding ratio is equal to 1 + w/s, as labelled in Figure 1.4. A folding ratio of 2 is equal to a fullness of 100%. The pleated drape model uses an approximation of the pleat geometry as a regular rectangular pattern. This allows for the entire pleated drape to be modelled using one repeat unit, similar to how venetian blinds are modelled. The radiation incident on a portion of the pleated drape fabric is absorbed, reflected or transmitted. If the radiation is transmitted or reflected it can then interact with other portions of the pleated fabric. Beam-beam reflection is considered to be zero, because this is the nature of drapery fabric, although beam-beam transmission through the open portions of the layer is considered. After the direct transmittance is calculated, the reflected and transmitted diffuse and beam-diffuse radiation is calculated using enclosure theory.

1.1.3 Thermal Calculations

Once the solar calculations are completed, thermal calculations must be performed. These determine both the U-value of the CFS, and the inward-flowing fraction of the absorbed

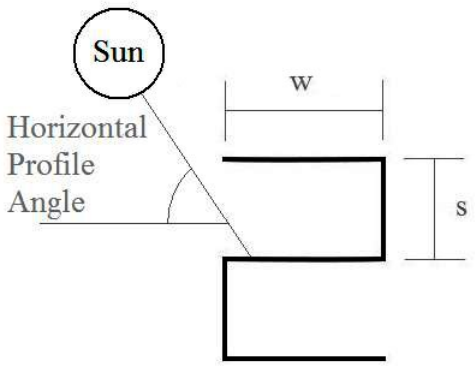

Figure 1.4: One repeat of a pleated drape, looking from above

solar energy, which is necessary for calculating the complete SHGC. Heat transfer is calculated separately for the centre-glass and edge-glass portions of the window. Center-glass heat flux is calculated as a 1-D heat flow problem, and uses a coupled analysis of conductive, convective and radiative heat transfer. Wright (1998) presents a centre-glass solution for windows composed of multiple glazing layers. It uses energy balances at the surfaces of each layer which are connected by the convective heat flow to the adjacent layers, the conduction through a glazing layer, and longwave radiation from the adjacent layer. This solution method treats convection heat transfer separate from the net radiation portion of the solution, and decouples the two modes of heat transfer. Although this solution method can be used for diathermanous layers,(Wright and Sullivan, 1987), this was not a large factor, as the only diathermanous layers of interest at the time of publication were thin plastic films. To solve for temperatures, a set of $4n - 6$ equations must be solved, where n is the number of layers in the CFS. This is an iterative solution, as the equations include convective coefficents and the emissive power of layers, all of which are temperature dependent.

1.2 Network Calculations

Wright (2008) proposed an efficient method of calculating heat flow through a CFS. This method uses a resistor network for both convective and radiative heat transfer. A portion of this general resistance network is shown in Figure 1.5. The resistor network allows for connections between any two layers, between any layer and the indoor or outdoor sides, and between the indoor and outdoor sides, in the unlikely event that direct indoor-outdoor heat transfer is possible. If the heat transfer coefficients are known in advance, the heat transfer coefficients associated with the resistors are used to form an energy balance on each layer. This results in $n + 2$ related equations. This set of equations is then solved for the temperature of each layer. This network solution method is the basis for the work done in this project.

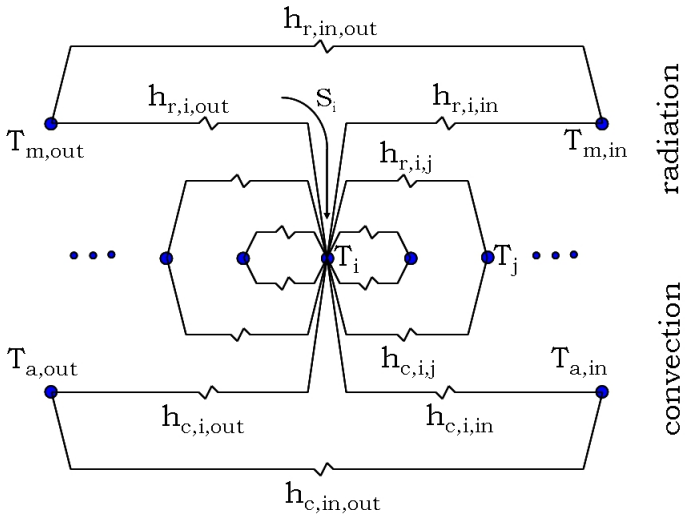

Figure 1.5: Heat flow paths considered by network model

Although the general network allows for connections to any layer, in practice not all the connections allow for heat transfer. For example, a solid glazing layer will stop any convection or radiation between layers on either side of it. An example of how the general network can be simplified and applied to a real system can be seen in Figure 4.5b.

Since it is more likely that the heat transfer coefficients are unknown, Wright (2008) also gives a method for calculating longwave radiant heat transfer coefficients. Since the

coefficients are temperature-dependent, this is an iterative process whereby an estimate of layer temperatures is used to calculate the first set of heat transfer coefficients, and then the layer temperatures are updated and are used to find the next set of heat transfer coefficients, until convergence is reached. To calculate the radiative heat transfer coefficients, the radiosity at each surface due to unit emission from another surface is calculated. To do this, radiosity energy balances are used to determine the radiosity of each surface due to reflection and transmission of unit emission from each of the surfaces. These are found through the solution of a system of $2n + 2$ equations for each surface. The resulting relative radiosities are used to calculate the radiative heat transfer coefficients.

Once the resistance network has been determined, in addition to being used to solve for the temperatures of the layers, it can be used to quickly determine the indices of merit for the CFS, since the indices of merit are dependent only on the resistance network, not on the temperatures of the layers. This sole dependence means that even if the environmental conditions change the indices of merit do not change, as long as the resistance network is held constant. The indices of merit are found using computational experiments, where the indoor and outdoor temperatures, and the insolation are set to convenient values, and each index of merit can be easily extracted.

To perform the computational experiments, the heat flow to the indoor side is determined using the resistance network for the environmental conditions of interest, with specially selected environmental conditions. To determine the heat flow to the conditioned space, heat flow from every layer to the inside must be considered.

$$q_{in} = (T_{a,out} - T_{a,in}) * h_{c,in-out} + (T_{m-out} - T_{m,in}) * h_{r,in-out} + \sum_{i=1}^{n} (T_i - T_{a,in}) * h_{c,i-in} + \sum_{i=1}^{n} (T_i - T_{m,in}) * h_{r,i-in} \tag{1.1}$$

For example, the U-value is calculated by setting the outdoor temperature to 1 and the indoor temperature and insolation to 0. The total heat flow is calculated using the known resistor set and Equation 1.1. The U-value is found using

$$U = \frac{q_{in}^{exp}}{T_{out}^{exp} - T_{in}^{exp}} \tag{1.2}$$

Since the temperature difference, $T_{out}^{exp} - T_{in}^{exp}$ has been set to 1, the numerical value of the heat flow to the indoor side, q_{in}^{exp} is the same as that of the U-value.

In addition to the U-value and SHGC, Wright (2008) presents computational experiments to determine $f_{r,in}$ and $f_{r,out}$. These are weighting factors to determine the contribution of the mean radiant temperature in determining the effective ambient indoor and outdoor temperatures.

$$T_{ae,in} = f_{r,in} * T_{m,in} + (1 - f_{r,in}) * T_{a,in} \tag{1.3}$$

One of the challenges with the general resistance network is to determine the temperature to be used for radiant exchange. Lomanowski (2008) describes the implementation of a network method for determining heat flow through windows in the framework of ESP-r. This method of implementing the network method deals with radiant exchange by taking the temperature of each surface in the room, and considering radiant exchange with that surface. This removes the need to calculate an indoor radiant temperature.

1.3 Other Simulations

Due to the aforementioned usefulness of computer models of complex fenestration systems, it is not surprising that several different simulation tools for windows exist. These include stand-alone programs to model fenestration systems, such as Window, WIS and FRAME-Plus, as well as window models in full building simulation programs such as ESP-r, eQuest and EnergyPlus. These different tools have different strengths and different abilities. A few examples have been described below, however there are many more options available, to fit different needs and meet different standards.

Tools designed to simulate windows alone generally calculate the solar heat gain coefficient, the U-value and some factor or factors describing the amount of solar visible radiation which is transmitted through the window. The primary differences between window rating tools stem from the standards which were used as the basis to develop the tool. Another factor which affects window simulations is whether the tool is intended to be used for comparison purposes, where various constructions are compared to each other, and only the relative values need to be known, or design purposes, where it is important that the indices reflect real-world situations. Full building simulation models aim at calculating the total energy usage of a building. This will include the heating and cooling loads, and in some cases will include the lighting requirements.

1.3.1 ASHWAT

ASHWAT is a joint project between the University of Waterloo and Wrightsoft Corporation[1]. It specialises in modelling complex fenestration systems with various types of shading layers. It uses equivalent layer properties, describing all layers with the same variable structure, so they can all be treated interchangably. Shading models from Kotey (2009) are used to determine the layer descriptions.

ASHWAT is separated into models for each layer type, a solar module and a thermal module. The layer models are used to determine the properties for each layer, the solar

[1] 131 Hartwell Avenue
Lexington,MA 02421
www.wrightsoft.com

module calculates the amount of solar energy which is absorbed in each layer or transmitted, and then the thermal module calculates layer temperatures and indices of merit. This is the framework that was used for the network model calculations.

The ASHWAT solutions rely on effective layer properties, which assume homogeneous behaviour. For something like a venetian blind, the amount of light transmitted will differ between the slats and the spaces between the slats. However, when looking at a large enough area, these inhomogeneities can be averaged out. ASHWAT calculates the centre-of-glass indices of merit for a window as well as the layer temperatures, heat fluxes, gap convective heat transfer coefficients and front and back longwave radiosities of each layer. ASHWAT does not currently track the location of solar visible light for daylighting calculations.

1.3.2 WINDOW and THERM

WINDOW is rating software for complex glazing systems, which is made available through the Lawrence Berkeley National Laboratories (LBNL). The current version is WINDOW 6.3 although version 5 is still available for download. It conforms to NFRC procedures and ISO 15099. It performs calculations for various standard sets of environmental conditions. THERM is a companion program for WINDOW, and calculates frame and edge-of-glass properties using a finite element analysis, with material information from libraries (Mitchell et al., 2011). WINDOW calculates the centre-of-glass window properties and combines them with the frame, divider and edge-of-glass properties calculated in THERM to determine the total window U and SHGC.

In addition to the indices of merit, WINDOW calculates the indoor and outdoor convective heat transfer coefficients based on indoor air temperature, fenestration height and wind speed and direction. It also calculates the condensation resistance, according to NFRC procedures. WINDOW uses spectral libraries to perform radiation calculations wavelength by wavelength and then weights the properties to obtain solar, visible and thermal transmittance..

1.3.3 WIS

WIS is a rating tool for windows, frames, shading devices and window components. It was developed by the WinDat European Thematic Network. The most recent version is 3.0.1 which was released October 2006. WIS offers users two different calculation modes. One mode is designed to strictly conform to draft European standards, and is intended for product comparison. It uses EN 410, EN 673 or ISO 10077-1 to determine calculation procedures and set boundary conditions. In this mode, WIS can calculate U-value, "solar factor (g-value), light and UV transmittance and general colour rendering index (Ra)" (WIS Help). It can calculate the U-value for a window with frame and surface temperatures of layers, to determine condensation risk, like WINDOW. However, when using WIS in this mode, no calculations can be done for windows with shading layers, or for off-normal incidence of beam radiation, as standards do not cover these cases.

The other mode available in WIS calculates according to physical principles. It allows user-defined conditions and the use of shading layers. User-defined conditions include different surface heat-transfer coefficients, not just ones defined in standards, thermally-driven or forced-air circulation and two different solar spectra, to accommodate different air masses. This mode calculates all the same properties as are calculated in the standards mode, but will do so in significantly more cases. In addition, off-normal layer properties can be calculated. Users have the option to select view-factor or ray-tracing methods for dealing with "scattering layers" such as venetian blinds, pleated drapes and screens.

1.3.4 FRAME^{TM}plus

FRAME^{TM}plus is a combined frame and glazing analysis program. It was developed by Natural Resources Canada together with Enermodal Engineering[2] (frame and edge-glass) and the University of Waterloo (centre-of-glass). The current version is an online tool, available through Enermodal at http://tools.enermodal.com/webframeplus/. It calculates SHGC, U-value, UV transmission, fading index and colour index for both the glazing area only and the entire window. The output includes performance specifications which can be

[2]582 Lancaster Street W,
Kitchener, Ontario N2K 1M3
www.enermodal.com

used in construction documents. Glazings are selected from a database of commercially available glazing layers and fill-gases are user defined. The user can also select the type of window – casement/awning, fixed or curtain wall. FRAME^{TM}plus does not include shading layers as part of a complex fenestration system, and only gives options for double or triple glazing (FRAME^{TM}plus Online information, FRAME^{TM}plus rating tool).

1.3.5 ESP-r

ESP-r is an open-source building simulation program with a world-wide development community. It is made available through the Energy Systems Research Unit of the University of Strathclyde in Glasgow. It simulates entire buildings and allows for high levels of detail in user specifications (Hand, 2010). The output can be tailored to the user's preferences. It relies on a finite-volume heat balance engine to analyse heat flow and energy requirements in buildings. Windows can be modelled as Transparent Multi-layer Constructions (TMCs) which both transmit and absorb solar flux. The multiple layers are thermally linked and the heat transfer between the layers and to the conditioned space is calculated as for any other construction. To model complex fenestration systems, the CFS construction as introduced by Lomanowski (2008) works in the same framework as the TMC for processing solar gains and transmitting heat, but includes slat-type blinds for solar and thermal shading in complex fenestration systems. More recent work by Joong (2011) allows for the use of other shading layers in the CFS construction, such as pleated drapes, roller blinds and insect screens.

1.3.6 EnergyPlus

EnergyPlus is a program available through the US Department of Energy. The current version is 6.0. It calculates building heating and cooling loads and total energy consumption. Windows are constructed in the standard user interface, and do not need to be fed in as pre-defined components from other window programs. The glazing calculations are layer-by-layer and are based on those from the WINDOW 4 and WINDOW 5 programs, however shading devices can be incorporated into the calculations. In addition to calculating heat flow through windows, EnergyPlus calculates daylighting of the indoor spaces to determine if the levels of artificial lighting can be reduced. In addition to allowing users

to build windows to be simulated, the program also takes inputs of indices of merit, which allows users to describe commercial products easily, as the U-value and SHGC will often be known even if a detailed layer-by-layer description of optical properties isn't available. A set of equations are described in the engineering reference manual (Boa, 2010) which detail the process by which an equivalent layer is created to match the specified the indices of merit. Angular performance of the glazing unit is estimated by comparing the combination of U-value and SHGC to those of other, known, glazing units, and the angular performance is modelled assuming the same behaviour of the most similar known glazing unit.

1.3.7 eQuest

eQuest is a building simulation tool made available through DOE-2. The software was developed by James J. Hirsch & Associates and Lawrence Berkeley National Laboratory. It is designed to be easy-to-use and not require a lot of experience, and has setup and output wizards, and provides 2D and 3D graphics of the building (DOE). Fenestrations can be dealt with in three ways - the first way simply uses a shading coefficient, a more accurate solution uses a predefined glass library, and for complex fenestration systems a layer-by-layer method is available for a limited number of windows. The layer-by-layer method can handle profile angle dependant slat-type shading layers, and shading layers in different positions, not just shades on the indoor side of the CFS (eQuestv3 – Overview). Output from eQuest varies depending on what reports the user chooses to run. In addition to outputting building information such as heating and cooling loads, and other energy consumption, eQuest allows parametric runs to examine the benefits of specific design features, and window information can be backed out from these reports.

1.4 Project Objectives

The goal of this project is to bring together work that had been done in several areas, and to integrate it into building simulation software. The network model is a more stable solution method, and the shading layer models to use with the model have already been developed. To be able to realise the full benefit from these models, it was necessary to be able to use them in building simulation software. While the models developed by Kotey (2009) have been implemented in ESP-r, they are not available with the network method, instead the native ESP-r solution methods are used.

This project integrates shading layer models with the network calculation, using the indoor and outdoor mean radiant temperatures. Indices of merit are calculated using the computational experiments of Wright (2008). In addition to the SHGC, U-value and radiant fractions, new computational experiments are developed to determine the cross-coupling coefficient and the radiant and convective fractions from each layer. These additional indices of merit are required for simulations which do not solve the entire network each time step. Calculating these values allows the window model to be solved once, and then the indices of merit used for several time steps, until the conditions change so much as to render the resistance network inaccurate.

The f_r indices of merit are simply measures of how much of the energy transfer, between the fenestration system and the environment, and between the fenestration system and the conditioned space, is by radiative heat transfer as opposed to convective heat transfer. This is useful in that it allows a single effective temperature to be used in place of the ambient air and mean radiant temperatures. The outdoor f_r is used as a weighting factor to combine the two temperatures: $T_{ae} = T_m(f_r) + T_a(1 - f_r)$. The indoor f_r can be used to separate the total heat flow into radiant and convective components. This is useful, because the two types of heat gain have different effects on the air temperature in the conditioned space, the cooling load and the timing of the peak cooling load.

The cross-coupling coefficient, C_x, is a part of the process used for certain simplifications of the general resistance network, namely when the network is simplified into a Delta circuit. Figure 1.6a shows the heat transfer paths, using an effective ambient outdoor temperature. If the heat flow into the conditioned space is desired in terms of the total convective and radiant heat flows, a Y-Delta transformation can be performed on the resistance network, giving the resistance network in Figure 1.6b.

Figure 1.6b shows that in addition to connections between the indoor temperatures and the outdoor effective ambient temperature there is a connection directly between the ambient air and mean radiant temperatures on the indoor side. This connection is the cross coupling coefficient, and determines how strongly ambient air and mean radiant temperatures affect each other. The same simplification can be made on more complex systems to give the convective heat flow, the radiant heat flow and the cross coupling coefficient. This simplification removes the need to solve the full network between every element in the conditioned space.

In addition to integrating the network model into building simulation, rapid and flexible fenestration models allow for the possibility of a stand-alone rating tool for complex fenestration systems. Another goal of this project was to develop a user interface for the network window model that could be used as a new version of the VISION tool (VISION5). Although VISION was a useful educational and rating tool, the most recent version of the program (VISION4) was a DOS-based program, and is not practical to use in Windows

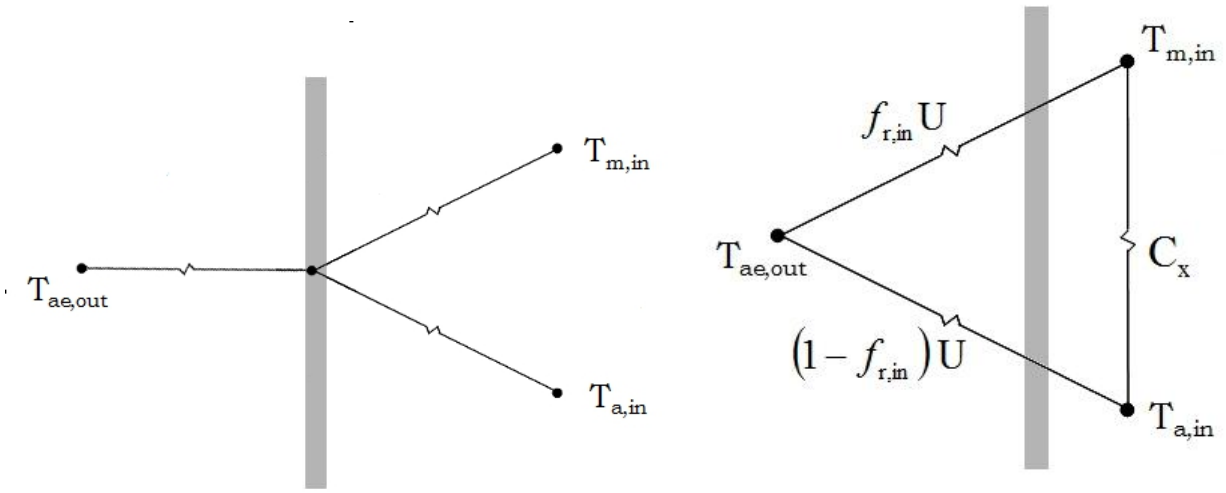

(a) Temperature connections using an effective outdoor temperature

(b) Equivalent delta circuit.

Figure 1.6: Y-Delta transformation for a single glazed window.

Vista and Windows 7. Additionally, an updated version of the VISION tool would be able to incorporate the flexibility of the network solution method, including the ability to incorporate multiple shading layers, or adjacent diathermanous layers. An easy-to-use and flexible tool for evaluating complex fenestration systems is useful for many reasons. The most practical and likely use of this tool is in education. A stand-alone rating tool can allow users to experiment with different constructions and to easily change one aspect of the window at a time. This would provide an easy way to learn how different components of the window interact, and how sensitive the indices of merit are to different kinds of changes. This is easier in a stand-alone tool, because the reduced number of calculations results in a much shorter wait than if an entire building is being simulated, and the information is directly available, and not buried in other building information. With the focus on the window, the user interface for editing the window can be drastically simplified, and any changes are obviously due to the window, not to incidental changes in the building. There is also potential that this tool might be a useful design tool on its own, although that is not a primary focus, as design is most useful when approached as a whole, rather than piecewise.

This project will develop several aspects of these options. It will examine shading layer models, specifically the measurement techniques used to develop them. The network model will be integrated into building simulation programs, and computational experiments to determine the cross-coupling coefficient developed. Finally, since the network model is very flexible, a stand-alone tool will be developed to model fenestration systems using the network model.

Chapter 2

Interfacing network calculations with building simulation

When creating building simulation programs, an important concern is the amount of time required to run a simulation. In a building with multiple windows, the window subroutine will need to be called for each window. This is in addition to the calls made to subroutines for other parts of the building, and whole-building calculations. These calls must be repeated for each time step. As simulations get more and more accurate, shorter, and therefore more, time steps are needed to model the building's behaviour over a year. This repetition of the calculations means that small changes in the speed of a subroutine can have a significant and important effect on the overall speed of the building simulation program. A poorly planned building simulation program can result in runtimes of hours or days. If building simulation is to be an integral part of the design process, runtimes of several days are not acceptable, so speed must be a priority. The strengths of the network model make it a better way to model fenestration systems, which should result in a decrease in solution times. This makes the inclusion of the network model in building simulation programs a high priority.

The network model was integrated into building simulation programs by modifying the ASHWAT modules so that the old thermal solution method was replaced with one using a network model. ASHWAT calculates the information which is needed for the building simulation and passes it to a handler program which co-ordinates the simulation. This means that the challenges with implementing the network model within the context of a building

simulation are ensuring that all the necessary information is calculated and is passed in the required format. Because the ASHWAT_Thermal module already interfaces with shading and solar models, the shading models as developed by Kotey (2009), and the solar model from Wright and Kotey (2006) can easily be used. The implementation discussed in this section deals specifically with the interfacing of this module with a simulation tool for the California Energy Commission, the California Simulation Engine or CSE. A summary of this implementation was published by Wright, Barnaby, Niles, and Rogalsky (2011).

Historically, building simulation and fenestration simulation have been two separate fields. Simple fenestration models were used in building simulations and were not as flexible or as detailed as the models used in stand-alone fenestration simulation. With the need to better simulate complex fenestration systems in the context of building simulations, this is starting to change. This change is not without difficulties, and one challenge in trying to integrate a formerly stand-alone fenestration model into a full building simulation program is in dealing with the radiant exchange between the conditioned space to the fenestration. When the ASHWAT model was integrated into ESP-r by Lomanowski (2008), this was handled by including individual parts of the fenestration network (i.e. resistors) in the building network which is managed by ESP-r, rather than solving the CFS separately from the rest of the building. In the CSE, this problem is handled by the use of a radiant temperature node, which represents the effective temperature of the surroundings. Radiant temperature gain is considered gain to this node.

The general resistance network (Figure 1.5) allows any layer to be thermally linked to any other layer and to the indoor and outdoor enviroments through convective and radiative heat transfer paths. This generality allows for heat transfer between non-adjacent layers, such as open channel flow between a blind and a glazing layer, connecting both the glazing and the blind to the conditioned space, or diathermanous layers in the fenestration system.

The resistors which make up the general resistance network are dependant on the layer temperatures. The layer temperatures are influenced by the environmental conditions, including the indoor and outdoor temperatures and the amount of incident solar radiation. However, the layer temperatures are dependant on the resistance network, and so an iterative solution is necessary. The absorbed solar radiation, however, can be determined directly, and so is calculated prior to beginning the heat transfer analysis. The solution method of Wright and Kotey (2006) is used to calculate the amount of solar energy absorbed in each layer. To begin, the optical properties of each layer are described using

terms of identical format, i.e. effective optical properties, without any differences based on layer type. The shading models developed by Kotey (2009) are used for this abstraction if the layer in question is a shading layer. This step must be done every time the network calculation is performed, as the beam solar properties of the layers are angle-dependant.

At this point the ASHWAT_Thermal calculations can begin. The first step in the calculation is to determine radiosities of each layer due to emission from other surfaces as described by Wright (2008) and in Section 1.1.3 of this document. This is only done once each time the module is called, as these values are not temperature-dependant, and so do not need to be recalculated with every iteration. Once these are calculated, the solution becomes an iterative process. First the convective heat transfer coefficients are calculated using the current estimates of layer temperatures. Although the network model considers a convective coefficient for each pair of layers, the convective coefficient is set to zero for any two non-adjacent layers. The exception to this is in the first and last gaps in the complex fenestration system. If the indoor gap is open to the room, then both the innermost layer and the next layer have convective exchange with the conditioned space. The innermost layer convects from both sides, and the next layer convects from the indoor surface. Similarly, an open gap on the outdoor side results in the outermost layer convecting from both sides, and the next layer convecting on the outdoor side. This is explained in more detail in Appendix C of ASHRAE RP-1311, which has been reproduced here with permission as Appendix B. With the exception of gaps vented to the indoors or the outdoors, convective heat transfer coefficients are all calculated as for a sealed cavity. If one of the layers is a venetian blind, an effective gap thickness is calculated using the width and angle of the slats, as well as a correction factor to better match how convection occurs with venetian blinds.

After the convective heat transfer coefficients are calculated, the radiative heat transfer coefficients are determined using the layer radiosities, emissivities and temperatures. Then the convective and radiative heat transfer coefficients are combined as per Wright (2008), and the set of equations, i.e. the general resistance network, is solved. This gives the temperature of each layer, from which the heat fluxes can be found. This process is repeated until the temperatures converge. Once the temperatures have converged, meaning that the energy balance at each layer is satisfied, the values of each component of the resistance network are known and can be used to solve for the indices of merit. Figure 2.1 shows the process followed by the network model.

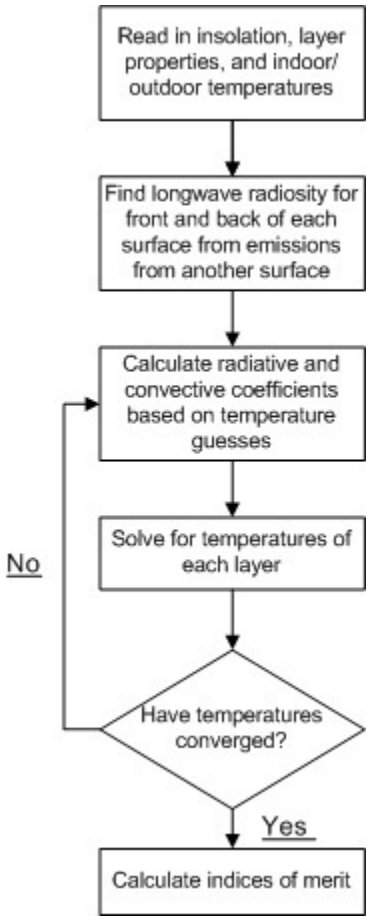

Figure 2.1: Program flow for network model

2.1 Indices of Merit

Conventionally, "incides of merit" refers to the U-value and the SHGC. For the purposes of this work, however, the meaning of the term has been expanded to include other measures which describe the thermal performance of the window. Just as U-value and SHGC are numerical values which allow the heat gain through the fenestration to be calculated, these other indices of merit are numerical values which allow other information to be found about the heat transfer characteristics of the fenestration system.

Computational experiments use the known resistance network to determine four indices of merit. In addition to the standard U-value and SHGC, $f_{r,in}$ and $f_{r,out}$ are calculated. As described in Section 1.2, $f_{r,in}$ and $f_{r,out}$ are weighting factors used to determine the effective ambient temperatures. These four indices of merit, together, can be used to quickly find the total heat gain of the conditioned space.

$$q_{in} = U_{cg} \cdot ((f_{r,out} T_{m,out} + (1 - f_{r,out}) T_{a,out}) - (f_{r,in} T_{m,in} + (1 - f_{r,in}) T_{a,in})) + \mathrm{SHGC}_{cg} \cdot I_{sol} \quad (2.1)$$

Indices of merit are obtained using computational experiments and the known resistance network for the complex fenestration system, as described by Wright (2008). To find the indices of merit, the total heat gain to the conditioned space for a given set of environmental conditions must be determined. There is no quick trick for finding the heat flow, and it must be determined by summing the heat flow from outdoors to the conditioned space, and the heat flow from every layer to the conditioned space. Many of these heat flow terms will be zero, but since the general network considers them, they must be included. To calculate the total heat gain to the conditioned space, the radiative and convective heat flows are calculated independently and then summed. The convective heat flow is

$$q_{c,in} = (T_{a,out} - T_{a,in}) \cdot h_{c,in-out} + \sum_{i=1}^{n} (T_i - T_{a,in}) \cdot h_{c,i-in} \quad (2.2)$$

and the radiative heat flow is

$$q_{r,in} = (T_{m,out} - T_{m,in}) \cdot h_{r,in-out} + \sum_{i=1}^{n} (T_i - T_{m,in}) \cdot h_{r,i-in} \quad (2.3)$$

As an example of a computational experiment, to determine the SHGC the inward-flowing-fraction, N_i, must be found for each layer. To do so, the indoor/outdoor temperature

difference is set to zero, and one unit of absorbed flux is introduced to each layer in succession. N_i is found for each layer by calculating the heat flow to the conditioned space. In addition to N_i, the generality of the resistance network allows the calculation of the radiative and convective portions of N_i. This is done by using Equation 2.2 and Equation 2.3 in two calculations in place of using Equation 1.1. These inward flowing fractions are referred to as $N_{a,i}$ and $N_{m,i}$, and are related to N_i through

$$N_i = N_{a,i} + N_{m,i} \tag{2.4}$$

The $N_{a,i}$ and $N_{m,i}$ sets are returned to CSE, along with τ_{sol} and the absorbed solar flux for each layer, S_i. The flux from insolation, S, which goes to each of the indoor temperature nodes is then calculated from Equations 2.5 and 2.6.

$$S_{a,cg} = \sum_{i=1}^{n} N_{a,i} S_i \tag{2.5}$$

$$S_{m,cg} = \sum_{i=1}^{n} N_{m,i} S_i \tag{2.6}$$

The reason for these extra calculations is due to the possibility of using a simplified resistance network, such as the Delta network used to represent the fenestration construction in the CSE calculations. The general, and more complex, resistance network for the CFS can be simplified to either the Y or the Delta form in Figure 1.6 by using $f_{r,out}$ to determine $T_{ae,out}$. The CSE uses the Delta form, so all heat flows to the conditioned space must be classified as either radiant, to $T_{m,in}$, or convective, to $T_{a,in}$. In addition the cross coupling coefficient, C_x, is required. This can be seen by the fact that the heat flow to the ambient temperature node in Figure 2.2 has two paths. A computational experiment for calculating C_x can be developed by considering the effect of C_x. If we look at the Delta circuit in Figure 2.2, we can see that C_x is a way to account for the effect that the mean radiant temperature has on the heat flow to the ambient temperature node and vice versa.

The cross coupling coefficient is evaulated with a numerical experiment since, like the other indices of merit, it is solely dependant on the values of the resistance network. The environmental conditions are set so that $T^{exp}_{a,in} = 0$, $I^{exp}_{sol} = 0$ and $T^{exp}_{m,out} = T^{exp}_{a,out} = T_{ae,out} = T^{exp}_{m,in} = 1$. Now, if we use the Delta circuit, we can determine that the heat flow to $T_{a,in}$

will be

$$q_{r,in}^{exp} = f_{r,in} \cdot U_{cg} \cdot (T_{ae,out}^{exp} - T_{m,in}) + C_x \cdot (T_{a,in}^{exp} - T_{r,in}) \tag{2.7}$$

Examining Equation 2.7, we can see that the first term is zero, since there is no temperature difference. All of the convective heat flow is through the cross coupling coefficient. Since the driving temperature difference across C_x is unity, the convective heat flux to the conditioned space and the cross coupling coefficient are numerically equal. This cross coupling coefficient applies to the true environmental condition, because the values for the resistance network which are used are those for the true condition, not those of the computational experiment.

Once the indices of merit are calculated, they are passed to the control function, and further calculations are done outside of the ASHWAT environment.

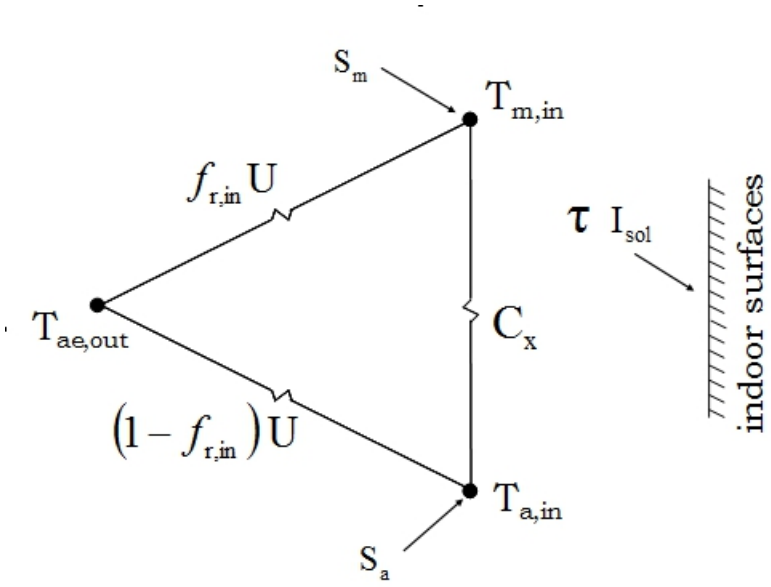

Figure 2.2: Delta form of the simplified network.

2.2 Flexibility

The generality of the network in Figure 1.5 means that it can describe any system, even if jump resistors are present. This in turn means that it can be used to find the indices of merit for any complex fenestration system, no matter what the composition. Even though the resistors are influenced by the layer temperatures, they are not as sensitive to changes in the environmental conditions as are the actual heat fluxes. Since the indices of merit are dependant only on the resistance network, they also are less sensitive to changes in the environmental conditions. To increase the speed of the calculations, the CSE takes advantages of this, and does not run ASHWAT_Thermal at every timestep. Instead, the indices of merit are calculated, and used to calculate heat flow into and within the conditioned space. The ASHWAT_Thermal module is called only when the ambient conditions have changed enough that the thermal resistance network for the complex fenestration system will have changed significantly.

To test the validity of reusing the indices of merit, a sensitivity analysis was carried out to evaluate the effect of small changes in environmental conditions on the indices of merit. This analysis consisted of calculating the indices of merit, and then changing one environmental input at a time by one unit, and re-calculating the indices of merit. The changes in the indices of merit were recorded in each case. This test was repeated with four different sets of initial conditions, which can be seen in Table 2.1. The entire test was repeated for several different fenestration systems. These tests confirmed that the indices of merit are insensitive to small changes in the environmental conditions. With the exception of when $h_{c,in}$ was changed, none of the indices of merit changed more than 5% due to a change in an environmental condition, and most changes were significantly under 1%. The indices of merit changed more in response to $h_{c,in}$ being changed, as a change of 1 $[\frac{W}{m^2 \circ C}]$ is a 33% change in the value of $h_{c,in}$.

Another advantage of the ASHWAT fenestration model is that it is flexible enough to allow the use of physical properties which are not accurate representations of possible conditions. This allows various approximations which can simplify and speed up the calculations. An example is setting the emissivity of the indoor environment to a value which is greater than 1. Although this is not physically possible, doing so allows for implementation of the Carroll methodology in calculating the mean radiant indoor temperature. The temperature of the radiant node is calculated through a weighted average of the temper-

atures of all the radiant surfaces in the room. This decreases the temperature difference between the indoor surfaces of the CFS and the radiant node, as the temperature of the radiant node is brought closer to the temperature of the indoor surfaces of the CFS by their inclusion in the calculation. To compensate for this, other driving factors in the radiant exchange between the nodes, such as the emissivity, must be increased, even if this requires a physically impossible emissivity. This adjustment is explained in more detail by Wright et al. (2011).

Finally, the flexibility of the general network means that diathermanous layers and open channel flow are handled more smoothly. Heat transfer between two non-adjacent layers is treated in the same way as heat flow between two adjacent layers. In the previous version of the ASHWAT model, open channel flow in a vented gap was handled in a different calculation than the rest of the heat transfer. Instead of calculating convective heat transfer from the two layers to the indoor or outdoor air and to each other, modified source terms were used at each layer to account for the open channel heat transfer, as described by Wright (1986). The problem with this setup is that the source terms were lagged one iteration, i.e. the solution was partially explicit, and this introduced instability. Because the network solution treats all the heat transfer in the same manner, the formulation is fully implicit and fully stable.

Table 2.1: Test conditions for sensitivity test. These represent the base case, and sensitivity to change was determined by changing one environmental variable at a time and recording the change in the indices of merit. This test was performed on multiple fenestration systems. (Barnaby, 2011)

Case	T_{in} $[^\circ C]$	$T_{m,in}$ $[^\circ C]$	T_out $[^\circ C]$	$T_{m,out}$ $[^\circ C]$	$h_{c,in}$ $[\frac{W}{m^{2\circ}C}]$	$h_{c,out}$ $[\frac{W}{m^{2\circ}C}]$	I_{sol} $[\frac{W}{m^2}]$
1	24	24	40	40	3	16	1
2	24	24	40	40	3	16	1000
3	20	20	0	0	3	24	1
4	20	20	0	0	3	24	1000

2.3 Testing and Validation

Testing for the previous version of ASHWAT, included a program to validate the output. As part of ASHRAE Research project RP 1311, this code was used to generate Indoor Attenuation Coefficients (IAC), used in simplified calculations to quantify the solar performance of shading attachments, for the 2009 ASHRAE Handbook–Fundamentals, and as such, there was a high standard of accuracy required. The calculation code was tested against all glazing systems previously in the ASHRAE handbook to ensure that the output matched. Although the shading models could not be compared to values in the ASHRAE handbook, similarly rigorous testing was done on them.

Since the new network solution was coded in the ASHWAT framework, validation could be done using the same program used to test the previous versions of ASHWAT. The only difference between the previous version and the network solution lies in how the layer temperatures are calculated. The same shading and convective models were used, so the two sets of results were of identical format, allowing for direct comparison. Since a correct solution would match identically, this made evaluation of the functionality of the program easier, as any mismatch in results indicated an error in the calculation.

Three cases were used for validation of the results from the ASHWAT fenestration model. The environmental conditions used for each of these cases are listed in Table 2.2. The first test is important for a basic preliminary check, as severe problems will be apparent if the temperature of the layers is not a constant $20°C$. Once this test case shows the stability of the solution, more complex test cases can be used. A test case with different indoor and outdoor temperatures allows for a more thorough test of the calculations. The temperatures were chosen to match the ASHRAE winter conditions. The convective coefficients differ from the listed h values for the ASHRAE winter condition because h for the ASHRAE winter condition is a combined coefficient for both radiation and convection. The adjusted values of h for the tests was calculated by taking an approximate value for the layer temperature and using that to determine the radiative heat transfer coefficient. This was subtracted from the ASHRAE h value, leaving a convective heat transfer coefficient. The final case allows not only for different temperatures on the indoor and outdoor sides, but for differing ambient air and mean radiant temperatures, as well as incorporating 600 $\frac{W}{m^2}$ beam insolation, and 75 $\frac{W}{m^2}$ diffuse insolation. This condition has the full complexity of a typical building simulation calculation.

The test program passes 13 different complex fenestration systems to the calculation modules. These are tested with each of the three abovementioned weather conditions. The tested systems include different gap types, different gap fill gases and different gap thicknesses. The systems were set up to test every type of shading layer, and combinations of multiple shading layers, and multiple adjacent diathermanous layers. The output from the test program for the new ASHWAT_Thermal code was compared to that of the old code, and results were matched to four or more significant digits.

2.3.1 Increased Speed

The speed advantages from re-using the indices of merit for multiple timesteps in CSE have already been discussed. Another feature offered to reduce the calculation time allows for the ASHWAT module to run, but to not iterate to solution. A set of initial temperature guesses are passed to the module, and the new heat transfer coefficients are calculated only once. When a good initial guess for temperature is available, this can cut run time for the module significantly. It is used for simulations with short time steps, where the temperatures from the previous time step are known to be similar to the current temperatures. If this option is used, it is necessary to periodically run the model to full convergence using the iterative solution, to ensure that the discrepancies don't become too large.

In addition to the speed savings available through calling the module less often, the new ASHWAT module has a speed advantage in its own run time. The previous version of ASHWAT required relaxation when open channel flow was present because of inherent instability. Although this relaxation increases stability, it comes at the expense of speed, as many more iterations are required to convergence. The increased stability of the network

Table 2.2: Conditions used for validation testing

Test Case	$T_{a,in}$ $[^\circ C]$	$T_{m,in}$ $[^\circ C]$	$T_{a,out}$ $[^\circ C]$	$T_{m,out}$ $[^\circ C]$	$h_{c,in}$ $[\frac{W}{m^{2\circ}C}]$	$h_{c,out}$ $[\frac{W}{m^{2\circ}C}]$	I_{sol} $[\frac{W}{m^2}]$
1	20	20	20	20	3	20	0
2	21.1	21.1	-17.8	-17.8	3.41	25.76	0
3	20	22	35	25	5	21	675

model removes the need for relaxation, and the number of iterations can be reduced, with an accompanying increase in speed. Any shading device on the indoor or outdoor side of a complex fenestration system, such as a roller blind, an interior venetian blind or a pleated drape, will have an open gap, and would require relaxation were the old solution method used. As most windows have some sort of shading device, whether for glare control or to reduce solar gain, time savings for modelling windows with shading devices will have a significant effect.

The test program recorded the number of iterations to solution, allowing confirmation that the network model does indeed require fewer iterations than the previous solution method. Both solution methods required only one iteration to solve for the layer temperatures in the first test condition (Table 2.2), with indoor and outdoor temperatures all set at $20°C$ and no incident radiation. For the more complex cases, both with and without incident radiation, the two solvers routinely took the same number of iterations, generally 3 to 5, to solve for the temperatures in a system when there were no open gaps. In a few of the cases the network model required one more iteration than the old solution method. These cases do not have any obvious similarities to which the extra iteration could be attributed, however none of these cases are likely to arise often since, as previously mentioned, none of them have open gaps. For systems with open gaps, the number of iterations is reduced by more than half - generally from 9 to 4 or from 8 to 3. The most dramatic difference was associated with a fenestration consisting of a double glazed window with an insect screen on the outside and a roller blind on the inside. The number of iterations required decreased from 61 or 62 to 3. This is a significant reduction, and confirms that there is a time savings in systems with open gaps. While there might be a slight time penalty in systems without open gaps, this would be only one extra iteration, compared to five or more eliminated iterations for open gap systems. Additionally, the prevalence of shading layers means that in simulations, the number of iterations will more often be reduced than increased.

Chapter 3

Integrating Sphere Modelling

To be able to implement the network model of a complex fenestration system, it is essential to know solar properties of shading layer materials, and in turn the effective layer properties. The work done by Kotey (2009) was essential, as it is the source of models for roller blind, insect screen and drapery materials. These models convert solar properties pertaining to normal incidence, which is readily available, to the corresponding off-normal properties, which are not as easy to find. The measurements which were used to develop these models used a novel technique to measure off-normal properties of materials. This technique used a sample holder inside an integrating sphere, to hold the samples at various angles relative to the incident beam. To learn more about this measurement technique, simulations were done of an integrating sphere with the sample holder inside.

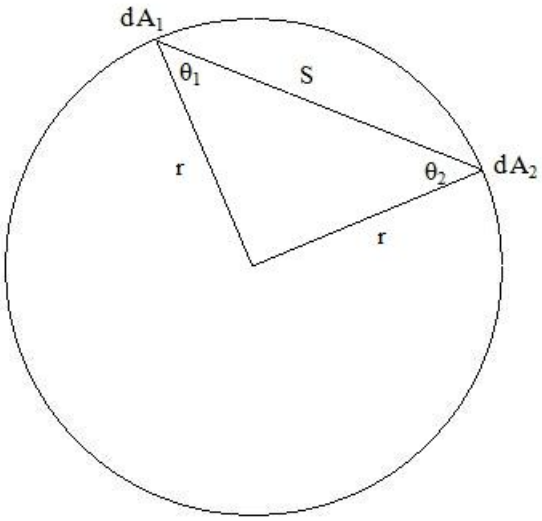

Figure 3.1: View factors in a sphere

3.1 Integrating Sphere Theory

The following derivation is being done in terms of flux and light levels. In an actual integrating sphere, measurements are taken wavelength-by-wavelength, however the theory is applicable to both cases and easier to understand in terms of flux.

To understand integrating sphere theory, we start with a theoretical sphere. The inside surface of this sphere has a highly reflective coating of reflectivity ρ_s, which reflects light in a Lambertian manner. This means that the intensity of reflected radiation is the same in each outgoing direction, independent of the direction of the incoming radiation. The inside of the sphere is perfectly uniform - there are no seams, ports or other irregularities. This sphere, of radius r, is shown in Figure 3.1, with the line of sight, S, between two differential areas on the surface of the sphere marked. The fraction of radiation which leaves one differential surface, dA_1, and arrives at another differential surface, dA_2 is given by Equation 3.1.

$$dF_{\text{d1-d2}} = \frac{cos\theta_1 cos\theta_2}{\pi S^2} dA_2 \tag{3.1}$$

where S is the chord between dA_1 and dA_2, and θ_1 and θ_2 are the angles between r and S, as shown in Figure 3.1. The length of S, between dA_1 and dA_2 is given by Equation 3.2

$$S = 2rcos\theta \tag{3.2}$$

Note that, by symmetry, $\theta = \theta_1 = \theta_2$

Combining Equation 3.1 and Equation 3.2, we get Equation 3.3:

$$dF_{\text{d1-d2}} = \frac{dA_2}{4\pi r^2} \tag{3.3}$$

Equation 3.3 makes it clear that the view factor between two points in the sphere is independent of the locations of the two points. This means that radiation diffusely reflected from any point on the sphere is spread evenly over the entire sphere. If we replace the differential areas dA_1 and dA_2 with finite areas A_1 and A_2, then it can be seen that the view factor from A_1 to A_2 is

$$F_{\text{1-2}} = \frac{A_2}{A_s} \tag{3.4}$$

where A_s is the total surface area of the sphere.

Next, continuing to assume that there is nothing interfering with reflections inside the sphere, picture a beam of light incident on the sphere as shown in Figure 3.2. The origin of this light is unimportant. A portion, ρ_s, of the beam will reflect and spread evenly over the entire surface. If the incident flux of this beam is $\Phi_i n$ and the cross-sectional area of the beam is A_c then the first reflection of this beam will result in a flux, given by Equation 3.5, incident over the entire inside of the integrating sphere.

$$\Phi_1 = \frac{\Phi_{in}\rho_s A_c}{A_s} \tag{3.5}$$

The second reflection will result in a flux, incident over the sphere, of

$$\Phi_2 = \frac{\Phi_{in}\rho_s^2 A_c}{A_s} \tag{3.6}$$

The flux from later reflections will continue to decrease in a geometric series. To find the total flux on the inside surface of the sphere, we sum the fluxes from each reflection and get

$$\Phi_t = \frac{\Phi_{in}\rho_s \frac{A_c}{A_s}}{1 - \rho_s} \tag{3.7}$$

Looking at Equation 3.5 through Equation 3.7, we can see that the flux incident on the integrating sphere is proportional to the cross-sectional area of the initial beam. After the

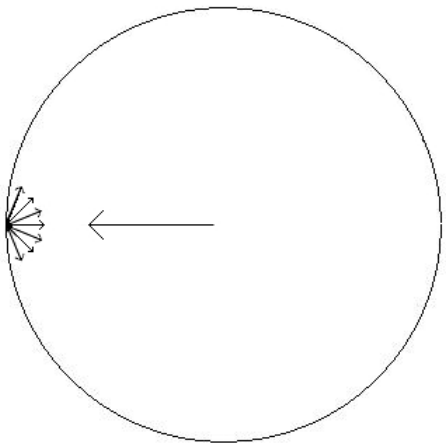

Figure 3.2: Light reflecting off the wall of a the sphere

first reflection, all that matters is the total amount of light [W or lm] which in this case is given by $\Phi_{in}A_c$, rather than the flux [$\frac{W}{m^2}$ or $\frac{lm}{m^2}$]. This is very important, since even if the source is spatially or directionally non-uniform, it is the total amount of light that is relevant, and this derivation still applies. Hence the name *integrating* sphere – the total amount of radiation over the area is measured, not the amount at any one point.

To measure surface properties with an integrating sphere there must be ports in the sphere, to allow the light to enter. These ports affect the reflecting characteristics of the sphere, as when light strikes the ports it is all lost. Following a similar derivation, we can see that once ports are added to the sphere, as in Figure 3.3, the flux on the surface of the sphere is reduced to

$$\Phi_t = \frac{\Phi_{in}\frac{A_c}{A_s}\rho_s(1-f)}{1-\rho_s(1-f)} \tag{3.8}$$

where f is the port fraction: $f = \frac{A_{ports}}{A_s}$. Looking at Equation 3.8, we can see that if we let $f = 0$, i.e. a case with no ports, Equation 3.7 is obtained. Conversely, if we let $f = 1$, i.e. the entire sphere surface is ports, then $\Phi_t = 0$, which is as expected, since all light incident on the sphere is lost, and so there is no reflected flux.

Looking at both the sphere without ports and the sphere with ports, the value of ρ_s is crucial. Although a change from $\rho_s = 0.98$ to $\rho_s = 0.96$ does not appear significant, we can see in the denominator that the absorptivity of the sphere coating, $\alpha_s = 1 - \rho_s$, plays

an important part. When ports are considered, this term is instead $1-\rho_s(1-f)$, however $(1-f)$ is generally close to unity, so α can still be considered to be present. In changing ρ_s by slightly over 2%, we have doubled the absorptivity. Hence Φ_t is very sensitive to even small changes in ρ_s. In a sphere without ports, Φ_t would decrease by more than half, from $\Phi_t = 4.9\Phi_{in}\frac{A_c}{A_s}$ to $\Phi_t = 2.4\Phi_{in}\frac{A_c}{A_s}$.

To use the integrating sphere as a tool for measuring optical properties, there needs to be a way to measure the amount of light which is being reflected in the sphere. For this, it is necessary to look at the radiance of the sphere surface. The radiance, L, of a diffuse surface due to an incident flux, Φ, is given by

$$L = \frac{\Phi\rho_s}{\pi A} \tag{3.9}$$

where A = the area of the diffuse surface. Combining Equations 3.8 and 3.9, we get Equation 3.10 which gives the radiance of the sphere wall (Labsphere, 2000).

$$L = \Phi_{in}\frac{\rho_s\frac{A_c}{A_s}(1-f)}{\pi A_s(1-\rho_s(1-f))} \tag{3.10}$$

When integrating spheres are used to measure the surface optical properties of materials, a common arrangement has a photosensor which measures the radiance of a portion of

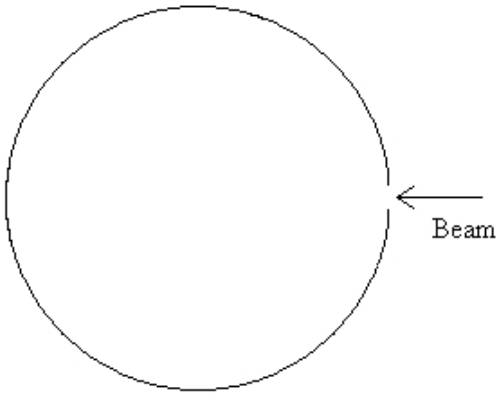

Figure 3.3: Integrating sphere with a port to allow an incident beam.

the surface. The ratio between the radiance of the measured surface to the light which is input into the sphere is the response of the sphere, R. This measurement is taken over a constant solid angle, effectively integrating the radiance over the surface seen by the photosensor. As long as the measurement is consistent, the actual angle over which the radiance of the sphere surface is measured is unimportant. Since the total amount of light is what matters, let us define the input such the surface area of the sphere and the surface area over which the sensor measures cancel out: $\Phi \frac{A_c}{A_s} \frac{\pi A_s}{A_{int}}$, where A_{int} is the area over which the sensor measures. This gives Equation 3.11 which gives a measure of the response of the sphere.

$$R = \frac{\rho_s(1-f)}{(1-\rho(1-f))} \tag{3.11}$$

3.1.1 Measuring Optical Properties

Figure 3.4 shows integrating spheres set up to take reflectance and transmittance measurements of material samples. The theory behind both types of measurements is similar so for simplicity, explanations will be given for reflectance only. To measure the reflectance of a sample, the sample is placed across the sphere from the entrance port, and a collimated beam of light shines on the sample, as in Figure 3.4a. The amount of light reflected in the first reflection is a fraction, ρ, of the incoming radiation. The characteristic of this first reflection will depend on the the reflecting characteristics of the sample. If the sample reflects in a Lambertian manner then the first reflection will be evenly distributed over the surface of the sphere. Otherwise, the first reflection will be non-uniform, and the light will not be uniformly spread over the surface of the sphere until the second reflection. It is often assumed that materials have both specular and diffuse reflection components. However, none of the shading materials which were tested have a specular reflection component.

Before an integrating sphere can measure reflectivity of a sample, a reference reflectivity is needed. This is determined through calibration of the integrating sphere, which sets the baseline for the specific geometry of the sphere and incident beam being used. Calibration also corrects for unwanted light, such as might result if the beam is not perfectly collimated. If the integrating sphere is changed in any way, aside from the sample itself, the calibration is no longer valid.

To calibrate an integrating sphere, four measurements are taken. Two of these measurements are for reflectivity and two are for transmissivity. The transmissivity reference measurements are simple to take. The first measurement is for 100% transmissivity, and involves taking a measurement with no sample in place, allowing all the light to enter the sphere. The second measurement is for 0% transmissivity, and is taken with an opaque cap used in place of the reference sample. The reflectivity measurements are taken at 0% reflectivity, with no sample in place, and the beam allowed to exit the sphere, and

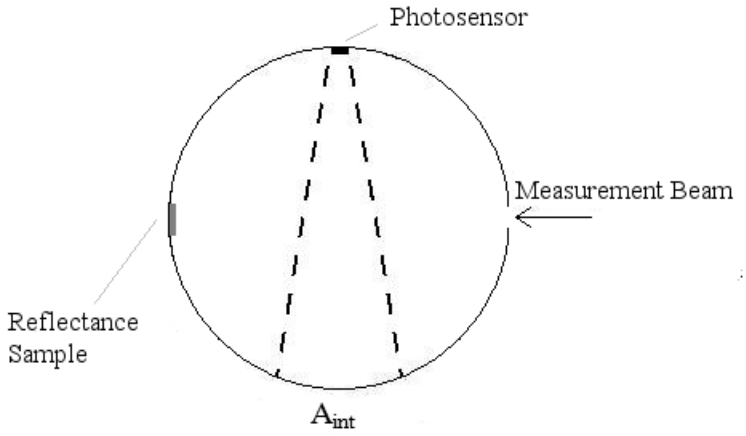

(a) Reflectance measurement

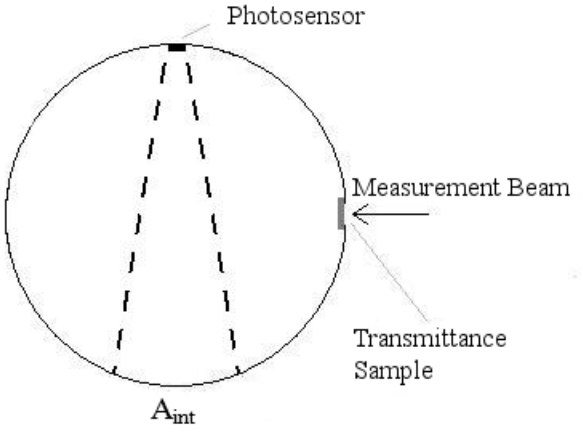

(b) Transmittance measurement

Figure 3.4: Integrating spheres used to measure reflectivity and transimissivity

at 98% reflectivity with a highly reflective sample using, in this case, the same material as the coating of the inside of the sphere. Ideally these reference samples should have the same directional characteristics as the samples to be measured, but this is not always practical. In the case of the work done by Kotey (2009), the measured samples had diffuse reflecting and transmitting characteristics. This was not a problem for the reflectivity calibration measurement, but the 100% transmissivty calibration measurement is specular. This means that the incoming light is not scattered over the entire surface of the sphere during the calibration measurement, whereas it is for the actual measurements. This is significant, because the diffuse light from the sample can be detected by the photosensor on the first reflection, but the beam from the 100% transmission reference can not be detected until the second reflection. The inaccuracy that occurs is relatively small and more detail can be found in work by Hanssen (1989).

One source of error which must be considered when using the integrating sphere for measuring surface optical properties, comes from the sample being measured itself (Goebel, 1967). This cannot be corrected with calibration, as the sample necessarily changes for each measurement. The sample replaces a portion of the highly reflective surface of the sphere with a material with a lower reflectance. This has a similar effect to adding ports – a portion of Φ_1, Φ_2 and of all subsequent reflections will be absorbed by the sample. This reduces the response of the sphere to R'. This could result in the reflectivity being underestimated, since $\rho R' < \rho R$. To compensate for the change in sphere response, a second incident beam is used. This reference beam is directed on a side of the sphere without being reflected from the measurement sample, as shown in Figure 3.5, and measures the changed response of the sphere. The output from this measurement procedure is a ratio of the measurement beam and the reference beam, such that output for a reflectance measurement is $\frac{\rho R'}{R'} = \rho$.

Another refinement in measurement techniques is due to the fact that the desired measurement is of the uniformly radiant sphere wall. It is important that the photosensor does not pick up any direct radiation from the source, or from the first reflection. To ensure that this does not happen, baffles are placed around the photosensor, as in Figure 3.6. The baffles block light which directly reflects from the measured sample from the photosensor, and allow calculations to be done with the assumption that the first reflection cannot be seen by the photosensor, so that the sphere response is uniform and proportional to the signal strength. As mentioned earlier, this may not always be an accurate assumption, but the associated inaccuracy is generally small (Collins et al., 2010).

Standard measurement techniques result in integrating spheres measuring the properties of a material at normal incidence. To adapt a standard integrating sphere to make off-normal measurements, angled sample holders that protrude into the integrating sphere to hold test samples at a known angle were developed (Kotey, 2009; Collins et al., 2010). The sample holders are shown in Figure 3.7, and the projection of a sample holder into an integrating sphere can be seen in Figure 3.6. This does not pose a problem in terms of measuring the response of the sphere, as the effect of a foreign body in an integrating sphere can be corrected through calibration (Nelson and Prézelin, 1993). However, the extent to which response of the sphere is changed by the presence of the sample holders is not known. This information is hidden by the fact that the integrating sphere is dual-beam, since the purpose of a dual-beam arrangement is that both the measurement and the reference beams are affected by absorbing surfaces, such as the sample holder. However, the absolute reduction in beam strength is significant as it can affect the signal-to-noise ratio. This chapter aims to examine the effect of the sample holder through the use of Monte Carlo simulations.

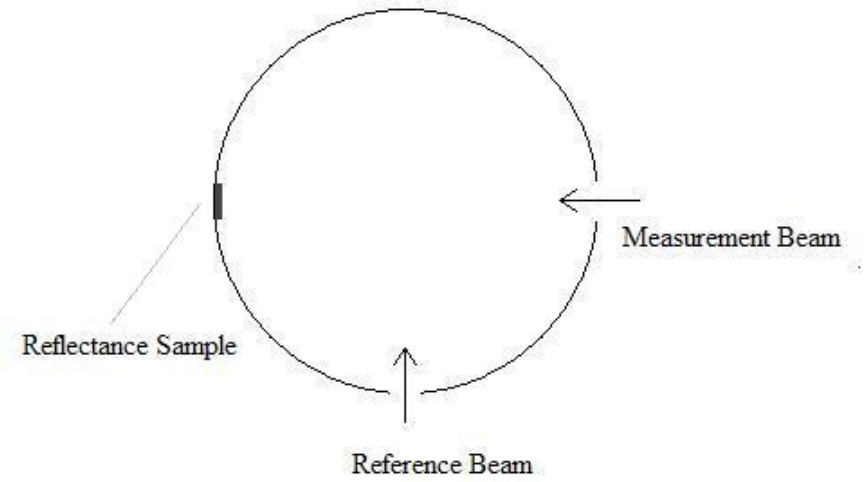

Figure 3.5: Dual-beam integrating sphere set up to measure reflectance, shown from the top. Only one beam is present at one time.

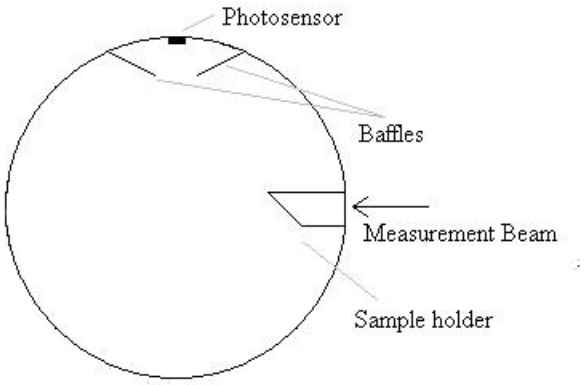

Figure 3.6: Integrating sphere with sample holder and baffles, set up to measure off-normal transmittance

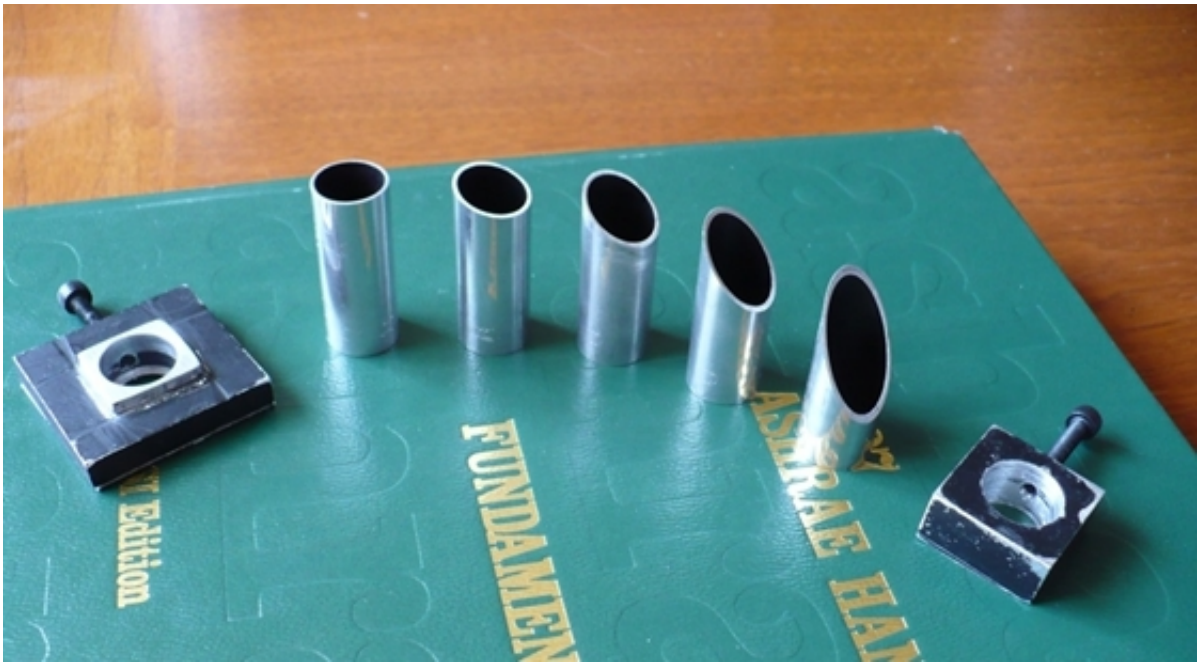

Figure 3.7: Sample holders used to measure off-normal properties

3.2 Methods of Analysing Integrating Spheres

Four methods for analyzing integrating spheres are presented in work by Clare (1998). These methods are the matrix method, summation-of-reflection, energy balance and integral-equation. These methods can be applied to different situations and require different amounts of computational power.

The energy balance method relies on the fact that the radiation is reflected evenly over the entire sphere, and does not differentiate between different portions of the sphere, beyond looking at the percentage of the area which is reflecting (Taylor, 1920). As such, this method is not well-suited for analysing spheres with irregularities, such as the sample holder.

The matrix method, summation-of-reflection and integral equation are all based on the idea that, when radiation is diffuse, the percentage of radiation leaving one point or surface and arriving at a second surface can be easily determined. This can be done using solid angles, as in the matrix method, or can be done with view factors which are simply known solid angle relations between two surfaces (Siegel and Howell, 2002). To apply the view factor relationships, the matrix method and summation-of-reflection separate the sphere into multiple zones between which the view factors are calculated. They require that irradiance and reflecting properties of the sphere be zone-wise uniform (Goebel, 1967; Tardy, 1991). This means that to obtain an accurate answer when non-uniformities are present in the sphere, a different zone must be used for each different level of irradiance or change in reflecting properties. Except in very simple cases, this is not practical, and so results obtained through these methods are approximate, due to the simplifying assumptions.

While the integral method does not implicitly divide the sphere into zones, the only ways to solve it are by dividing the sphere into uniform zones or using a numerical solution (Jacquez and Kuppenheim, 1955), which results in the sphere once again being divided into zones, with the associated approximations.

3.3 Monte Carlo

Unless the reflections are not diffuse, the inaccuracies associated with the aforementioned methods are small (Jacquez and Kuppenheim, 1955). However, as all of these methods make assumptions of zone-wise uniformity, they are not useful for checking the effect of this assumption. If a different approach to analysis is desired, a Monte Carlo simulation can be used to provide a picture of what happens inside a sphere when baffles are present (Keef et al., 2008) or for other modifications to the simple spherical geometry. Monte Carlo does not require making approximations, so the results from it will be as accurate as the geometric and spectral characterisation of the integrating sphere. In addition to simulating non-uniform radiation, Monte Carlo simulations can simulate an integrating sphere where the reflectivity of one or more surfaces is non-Lambertian (Prokhorov et al., 2003; Hanssen, 1996).

To perform a Monte Carlo simulation for radiation analysis, the paths of bundles of photons are traced. These photon bundles are treated as rays which travel in straight lines only. The intersection of each bundle with the surfaces within the sphere is calculated. When the photon bundles strike a wall, the photons are either absorbed or reflected. With a large enough sample size, the outcome of the simulation will be accurate(Burns et al., 1990).

Since Monte Carlo simulations allow for calculations to be done both with and without simplifying assumptions, they provide an effective way to check the validity of these assumptions. They are also useful when results cannot easily be experimentally verified. In these cases, Monte Carlo simulations can be used as a comparison for analytical solutions.

3.4 Simulation

For this simulation, ray-tracing was used to determine the paths of bundles of photons. Two different measurements were simulated, one for the measurement beam and one for the reference beam. For each of these simulations, photon bundles were emitted as from a collimated point source at the centre of the port of interest, travelling through the centre of the sphere to the far side. When the photon bundles strike a surface, a random number between 0 and 1 is generated. If this number is less than the reflectivity of the surface, the photon bundle is reflected. Its new direction is randomly determined assuming diffuse reflection from the surface. This procedure is repeated until the photon bundle is absorbed or exits through a port. The initial reflection does not use an algorithm with uniformly distributed directions for the first reflection, such as the shadow rays algorithm used by Ohno (1994), but, in a more general manner, is treated as any other reflection.

The sphere which was described in this simulation was selected to match the sphere used in the experiments, which is shown in Figure 3.8, as closely as possible (Kotey, 2009; Collins et al., 2010). The physical layout of the sphere is the same as that shown in Figure 3.6. It is a dual-beam integrating sphere, with a diameter of 110 mm. The inside of the sphere has a reflectivity of $\rho_s = 0.96$. The port through which the measurement beam enters has an area of 779 mm^2. The port through which the reference beam is enters has an area of 146 mm^2. The combined surface area of the sphere which is lost due to these two ports is 925 mm^2, or 2.4% of the surface area. The seams down the centre of the sphere and around the reflection port were neglected. Baffles shield the photosensor and were modelled as flat surfaces. One baffle is on either side of the photosensor, similar to the sphere in Figure 3.6. When a sample holder was used, it was modelled as a cylinder with a radius of 15.75 mm and a projection of 30 mm into the integrating sphere. The end of the sample holder was modelled as having a 0° angle. The surface of the sample holder was modelled as a diffuse surface with various reflectivities.

For these simulations, the strength of the signal was determined by counting the number of photon bundles which were reflected up from the bottom portion of the sphere. This was done by counting any photon bundle which originated below the imaginary surface shown in Figure 3.9. This imitates the integrating area which is also shown in Figure 3.9.

To determine the number of photon bundles required for an accurate simulation, the most complex case was simulated with increasing numbers of photon bundles until the

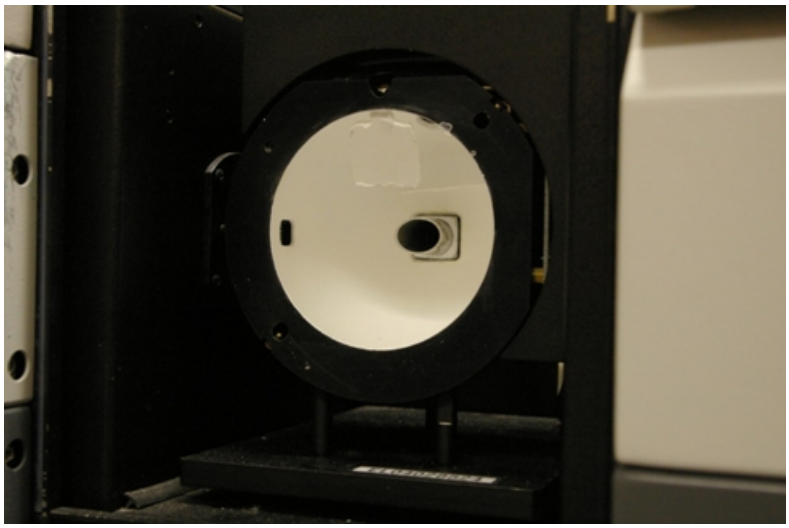

Figure 3.8: Integrating sphere used in initial measurements of Kotey et al. The simulated sphere was based on this geometry. A sample holder is in place, and the port for the reference beam can be seen on the left wall. The photosensor is at the top of the sphere, behind the baffles.

desired uncertainty was reached. The bundles were distributed evenly across twenty simulations. To determine the result to within 0.1% with 95% confidence, 6 400 000 total bundles were used. This number of bundles was used for all cases.

To validate the models used in the simulation, a first simulation was done with a perfectly uniform sphere without entrance ports, baffle or sample holder. In this scenario every point on the sphere receives completely diffuse irradiation and the radiosity distribution over the surface is uniform. To this base simulation, ports of varying area were added, and the change in response was compared to the theoretical change in response calculated using Equation 3.9. The results of this comparison are shown in Figure 3.10. This shows that the simulated results match theory exceptionally well, and demonstrates the effect that ports openings have on the signal strength.

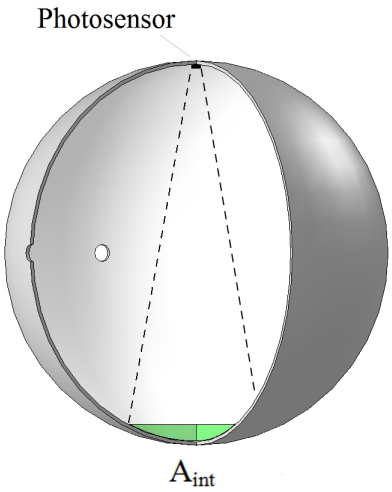

Figure 3.9: Imaginary surface at the bottom of the integrating sphere used to determine radiance of measured surface.

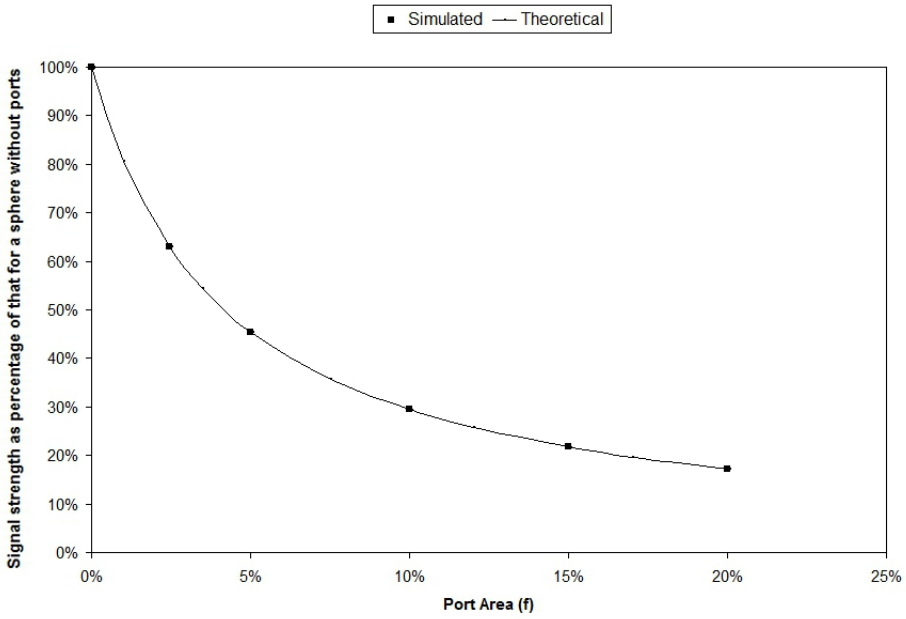

Figure 3.10: Results of validation simulations. Note that the theoretical and simulation results agree extremely well. The uncertainty of the simulated results is $\pm$ 0.22%

3.5 Results and Discussions

The original experiments to test the effect of the sample holder tube tested sample holders with reflectivities of ρ_{tube} =0.8 and ρ_{tube} =0.05 (Collins et al., 2010). These were chosen as practical extremes of reflectivity. To achieve ρ_{tube} =0.8, a highly polished metal tube was used. This is the sample holder type that was used in the measurements of Kotey (2009). The lower reflectivity, ρ_{tube} =0.05, was achieved by painting the surface of the sample holder with flat black paint.

In addition to the tested reflectivities, sample holders of two other values for ρ_{tube} were simulated. These were ρ_{tube} =0.96, representing a theoretical highly reflective surface, to match that of the integrating sphere, and ρ_{tube} =0.5, an intermediate value which would be typical of a unpolished metal sample holder. Of the four values for ρ_{tube}, three of them would only be present on diffusely reflecting surfaces, and only the highly polished metal would have specular reflection characteristics. The surfaces of all sample holders were simulated as having Lambertian reflection characteristics in order to solely examine the effect of ρ_{tube}. Simulations for all four tube reflectivites were done both with and without baffles, to look at the effect of the baffles, since baffles are frequently neglected entirely when analysing integrating spheres. The results from these simulations can be seen in Table 3.1.

The measurements done on the integrating sphere to measure the effects of the presence of a sample holder used an integrating sphere which had been calibrated without a sample holder in place. The simulated "Signal" values are reported as a percentage of the value for the sphere without a sample holder in place to simulate this, as shown in Equation 3.12 for the measurement beam and Equation 3.13 for the reference beam.

$$\text{Signal}_{meas} = \frac{n_{meas}}{n_{meas}^{no\,tube}} \tag{3.12}$$

$$\text{Signal}_{ref} = \frac{n_{ref}}{n_{ref}^{no\,tube}} \tag{3.13}$$

where n is the number of bundles counted as part of the signal strength.

The calibration measurement is defined as 100% signal strength, and replicates the 100% transmission measurement for calibration, so any output from the integrating sphere will be scaled by that measurement.

Because the experimental values to which these simulations must be compared have only the reported transmission measurements to compare with, the transmission measurement which would be reported for each simulation is calculated. If the sample holder tube had no effect, this value would be 1, as there is no sample through which the beam is transmitting. The values in the "τ_{rep}" column were calculated by taking the ratio of the signal for the measurement and reference beams, as shown in Equation 3.14.

$$\tau_{rep} = \frac{\text{Signal}_{meas}}{\text{Signal}_{ref}} \tag{3.14}$$

If we substitute Equation 3.12 and Equation 3.13 into Equation 3.14, then we get Equation 3.15

$$\tau_{rep} = \frac{n_{meas}/n_{ref}}{n_{meast}^{no\,tube}/n_{ref}^{no\,tube}} \tag{3.15}$$

It should be noted that the $n_{meas}^{no\,tube}/n_{ref}^{no\,tube}$ term in the denominator of Equation 3.15 is constant for a given geometry – either with or without baffles. This is because the calibration of the integrating sphere is the same for each series of tests, no matter what the reflectivity of the sample holder.

Examining Table 3.1, and comparing the measurements taken with and without baffles, it can be seen that the presence of the baffles makes very little difference and can safely be neglected.

Table 3.1: Monte Carlo simulation results. Estimated uncertainty is ± 0.1

	With Baffles			Without Baffles		
Case	Signal_{meas}	Signal_{ref}	τ_{rep}	Signal_{meas}	Signal_{ref}	τ_{rep}
No Tube	100.0%	100.0%	100%	100.0%	100.0%	100%
$\rho_{tube} = 0.96$	93.8%	94.8%	99%	93.7%	94.8%	99%
$\rho_{tube} = 0.80$	79.9%	80.2%	100%	79.9%	80.1%	100%
$\rho_{tube} = 0.50$	63.6%	63.1%	101%	63.4%	63.0%	101%
$\rho_{tube} = 0.05$	50.2%	48.8%	103%	49.9%	48.7%	102%

Looking at the τ_{rep} columns, we can see that when a high reflectivity sample holder tube is present the reported transmissivity is slightly lower than 1. This agrees with the experimental results, which found that the presence of a sample holder tube decreased the reported transmissivity.

One surprising result is that the trend as ρ_{tube} decreases is for the output to increase rather than decrease. This makes some sense, as the first reflection of the measurement beam will not be intercepted by the side of the sample holder tube, but the first reflection of the reference beam will. This should result in more of the photon bundles being absorbed by the sample holder tube when the reference beam is simulated than when the measurement beam is simulated. Figure 3.11 shows the first reflections of the measurement and reference beams with a sample holder in place, demonstrating that the first reflection of the reference beam will encounter the sample holder. To test this theory, the number of bundles absorbed by the tube was recorded and is shown in Figure 3.12. There are more bundles absorbed from the reference beam than from the measurement beam, and so it is unsurprising that the reference beam undergoes more attenuation than does the measurement beam. However, this trend does not match the experimental results reported by Collins et al. (2010), and more simulations and experimental measurements are needed to understand the discrepancy in τ_{rep}.

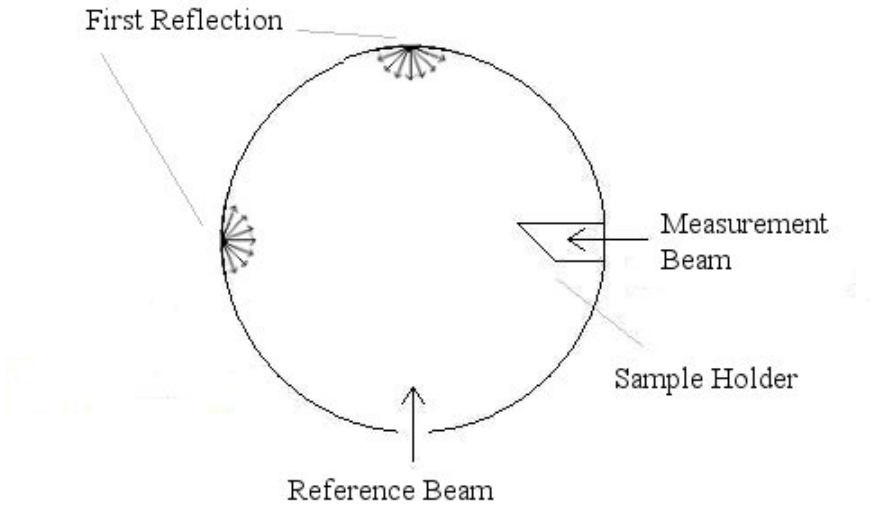

Figure 3.11: First reflections from measurement and reference beams. Note how the first reflection from the reference beam will interact with the side of the sample holder, while the first reflection from the measurement beam will not.

A signal strength reduction of 60% was predicted by Collins et al. (2010) for a black-painted sample holder with ρ_{tube} =0.05, and of 20% for a sample holder with ρ_{tube} =0.85. As the simulated reduction in signal strength is 50% for the sample holder with reflectivity of 0.05, and between 6% and 20% for a sample holder with reflectivity between 0.96 and 0.80, there is good agreement between these analytical solutions and the Monte Carlo results.

Although the effect of the sample holder tube is largely corrected by using a dual-beam sphere and the remaining effect can be removed by calibration, there is clearly a substantial signal reduction as the reflectivity of the sample holder tube decreases. If the beam reduction is too great, this can adversely affect the signal-to-noise ratio in measurements from the integrating sphere, especially in cases when the sample being measured has a very low transmissivity or reflectivity. Care should be taken to take a sufficient number of samples to compensate for the reduced signal-to-noise ratio.

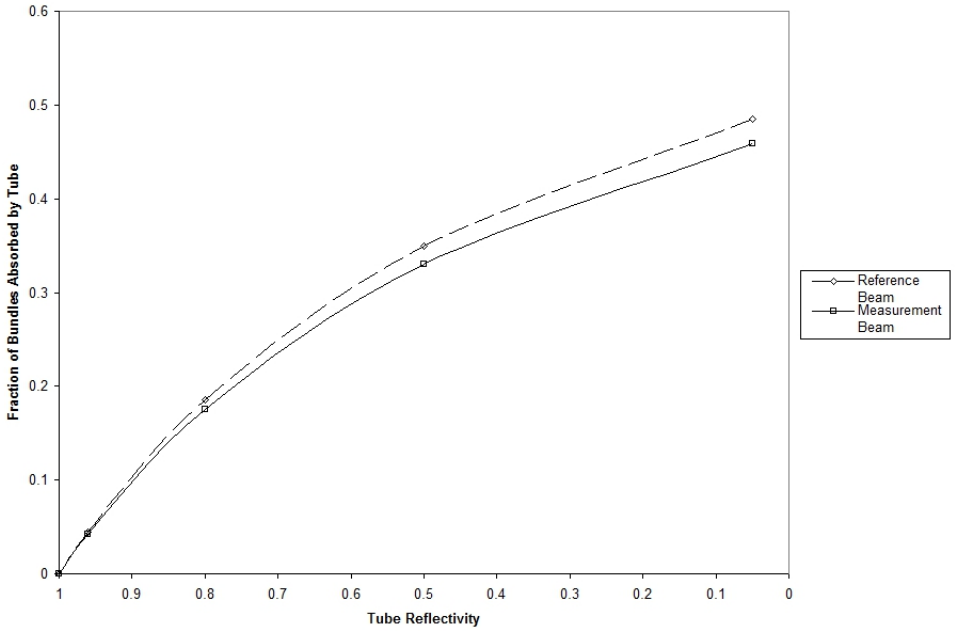

Figure 3.12: Number of bundles absorbed by the tube.

3.6 Conclusions

Although it is difficult to experimentally measure the effect of a sample holder tube, Monte Carlo simulations show that the presence of a sample holder tube can appreciably reduce the signal strength. This observation is in good agreement with radiosity calculations which were performed.

Sample holder tubes have more effect on the reference beam than on the measurement beam, although the effect is small, making it essential that the integrating sphere be calibrated with the sample holder in place.

Additional simulations should be done. This would allow the sample holder with ρ_{tube} =0.8 to be more accurately simulated, using specular reflection characteristics. As this is the sample holder that was used in later experiments, it is the most important case to understand well. In addition, more experiments and simulations should be done to understand to discrepancy between the calculated τ_{rep} from the Monte Carlo simulations and τ_{rep} from the experiments. This will further explain the effects of a sample holder tube in the integrating sphere, and allow better confirmation of the results from the Monte Carlo simulations.

The reflectivity of the tube surface has a large effect on the beam attenuation. The more reflective the tube, the less its presence reduces the response of the sphere.

Chapter 4

Rating Tool

Although modelling energy flows in buildings is useful, there is also demand for stand alone simulation tools for windows. Stand-alone tools allow different complex fenestration systems to be compared to each other for rating purposes or evaluated for design purposes. Due to the usefulness of stand-alone tools, a user interface was developed to be used with the new ASHWAT network solution to form a rating tool. The rating tool is designed so that a user can easily and quickly calculate the indices of merit for various complex fenestration systems. Users can build complex fenestration systems and set weather conditions. Once the user has constructed a complex fenestration system in the GUI, the information is parsed and passed to a DLL created from the Fortran code. The indices of merit are then calculated, and the temperature, solar absorption and heat flow are shown graphically. The primary goal of this rating tool was educational, so that people can quickly and easily compare the effects of different shading layers and different combinations of shading layers. The desire for stand alone fenestration simulation tools is confirmed by the positive response when this rating tool was presented at the 2011 ASHRAE summer conference in Montreal.

4.1 User Interface

The user interface, shown in Figure 4.1, is strongly influenced by the way the network calculation is performed. The information is presented in a manner similar to the way it is used for the calculations. In both the ASHWAT calculation engine and the GUI, the complex fenestration system is treated as an object, made up of two arrays - one of layers such as glazing layers or shading devices, and one of gaps to describe the spaces between layers. These two components are the basis for how the user describes a complex fenestration system. Each component is independent of the others – a double glazed window is treated instead as two glazing layers and a gap, any of which can be changed independently. This is why for any layer or gap the user can make changes by left clicking, and can view the current properties by right clicking, while pointing the mouse at the object of interest. This simple and uniform approach was chosen in part to make the rating tool easy to use, so that new users could quickly learn how the program works just from using it. In a similar vein, as much information as possible is communicated using pictures that update as the user makes changes, so that the user gets immediate feedback and can easily see the result of the change. In addition, the use of pictures makes it easier for users who do not have a strong command of the English language to understand the interface. Although the user interface currently limits the user to no more than eight layers, this can be changed in the software settings, and is not a limitation of the solution method.

When changing layers, users are restricted to predefined layers in libraries. The library files vary with the layer type, and contain the information needed to construct a model of that layer. For example, a venetian blind library file contains the slat solar transmittance and reflectivity, the slat longwave transmittance and emissivity, the slat thermal conductivity and geometric information about the venetian blind - the slat width, spacing and crown height. By freezing the layer definitions within the program, accidental changes to the layer properties can be prevented. The user has access to comprehensive libraries of layer types, and in addition to selecting a new layer or layer type from the library, if a user wishes to model a layer which is not included in the library they can add an entry to the library files. The distribution package includes template files for each layer type, so that users can see how to format library entries. The libraries for glazing layers contain commercially available glazings, taken from the IGDB[1], which is updated with information

[1] http://windows.lbl.gov/materials/IGDB/

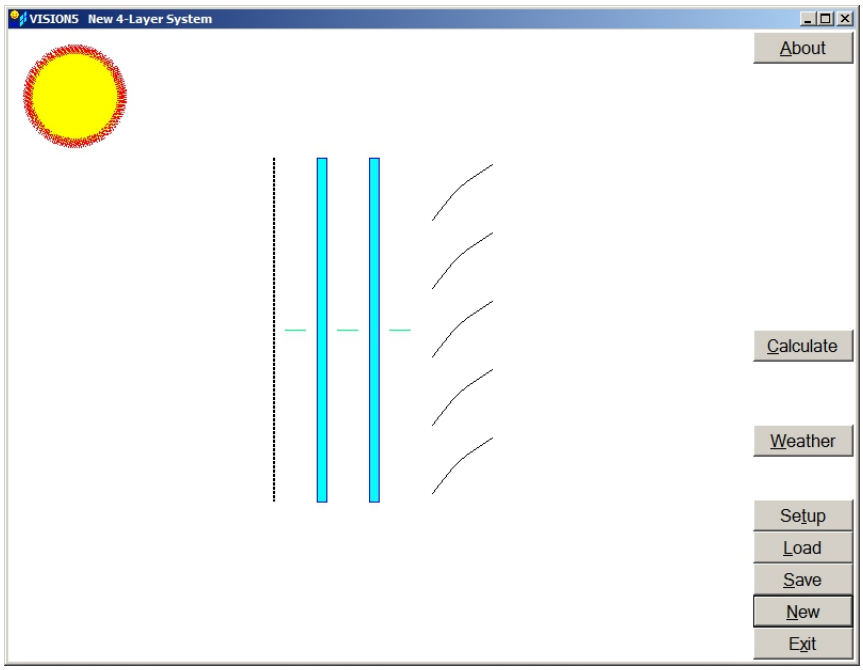

Figure 4.1: GUI showing a diagram of a system with four layers: an insect screen, two glazing layers and a venetian blind.

provided by glazing manufacturers, so it is likely that any commercially produced glazing layer will already be available. Libraries for shading layers have been constructed to be representative of common shading devices.

A few details about some of the layers are user-controlled. These are geometric details which prevent the need to store excessive layers. Specifically, users can flip a glazing layer to reverse the front and back properties, adjust the folding ratio of a pleated drape or adjust the slat angle for a venetian blind. These are easily accessed through the same control which allows users to select a new layer from the library, putting all the layer editing features in the same location. Being able to edit the geometric properties of the shading layers highlights the fact that the same computational routines, when used in building simulations, allow for on-the-fly control of these shading layer features, particularly venetian blind slat angle.

To examine a layer, the user right-clicks on the layer. A window pops up and displays the layer information. Each different layer type has a different information window, and gives different types of information. The dialogue for a venetian blind layer is shown

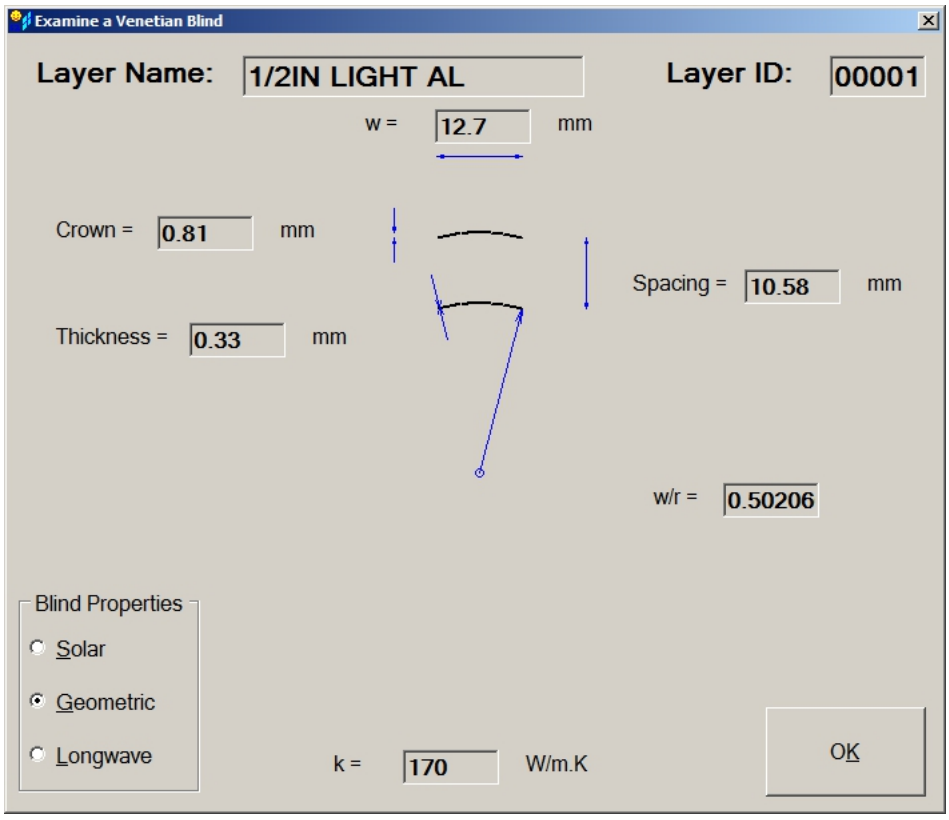

Figure 4.2: Dialogue to examine the properties of a venetian blind. Note the options to switch to viewing solar or longwave properties.

in Figure 4.2. The information windows have an image of a typical layer of that type and up to three sets of information: the geometric, solar and longwave properties of the layer. Only one property set is displayed at a time, as this prevents confusion between the longwave and solar properties. The optical properties are identified through arrows, with single arrows showing beam radiation (solar only), and fan arrows showing diffuse properties. These allow the user to confirm the layer properties.

Unlike layers, gap properties are user-controlled. The user can set the width of the gap as well as the type. The gap type controls whether the gap has open channel flow, vented to either the indoor or outdoor side, is an evacuated gap or a stagnant gap (no fill gas motion, resulting in only conduction through the fill gas), or a standard sealed gap with convection between the two layers. If the gap type is set to a sealed type - either the

default gap with convection, or a stagnant gap - then the user can also adjust the fill gas composition. The user can select percentages of five different gases for the composition of the fill gas: air, argon, krypton, xenon and SF6. In addition, users can import a sixth gas. This can be any gas of the user's choosing if they have created a definition file for it. Just like with the layer libraries, a sample gas definition file and template are available.

One thing the user interface does not do is check the feasibility of the complex fenestration system. For example, the rating tool allows the fill gas mix in the gaps on either side of a Venetian blind to be different. Checking is performed only on percentages such as for gas mixtures in gaps, or for the split between different types of insolation. This puts an onus on the user to check the construction of the system to ensure that the system is realistic. However the decision was made to not limit the freedom of the user to explore unusual design features.

The user interface gives the option of saving the complex fenestration system. This saves the layer and gap data, including drape fullness, venetian blind angle and fill gas composition for each gap. If a user-defined gas has been loaded, it is included in the save file. The definition file for a user defined gas is not required to open a system which includes a user defined gas, it is loaded from the save file. Save files can be opened again in the rating tool. Weather conditions are not saved, and will have to be set again. If the user selects the correct format, save files can also be used in ESP-r.

Another area over which the user has control is the weather. The user can specify the solar angle in terms of elevation angle and wall-solar azimuth angle. For the amount of insolation, the user specifies the total flux on the window and what percentage of the flux is beam radiation, diffuse radiation and diffuse radiation from the indoor side. Alternatively, the user can choose to numerically specify flux amounts for each of the three types of radiation. In addition to specifying the solar radiation, the user describes the temperature. The ambient air and mean radiant temperatures for both the indoor and the outdoor sides can be independently specified. As can be seen in Figure 4.3, the effective ambient temperature is marked with a horizontal dash. The mean radiant temperature is circled, and is connected to the nearest layer temperature with a dashed line. The ambient air temperature is connected with a solid line, the curve of which is determined by the magnitude of the convective heat transfer coefficient.

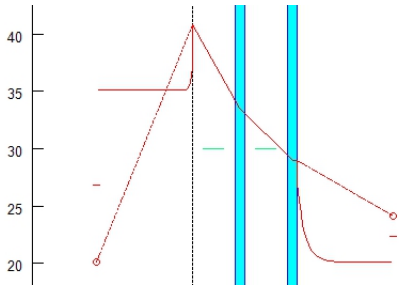

Figure 4.3: The ambient air and mean radiant temperatures are both shown when the results are displayed.

Indoor and outdoor convective heat transfer coefficients can also be individually set. To simplify the procedure for the user, the rating tool also offers the option to set the solar radiation and angle, temperatures and convective heat transfer coefficients to the ASHRAE winter or ASHRAE summer conditions with the click of a single button. The temperature conditions are not saved if the user saves the complex fenestration system, but do persist in one session if a new fenestration system is loaded or created. This persistence is another featured intended to facilitate comparisons.

4.2 Calculations

When the user finishes creating or loading a complex fenestration system, and sets the weather, the analysis can be undertaken. The rating tool performs the job of the wrapper program and controls the order of calls. First the effective solar properties of each layer are calculated, using the models from Kotey (2009), and these effective layer properties are combined with the absorbed solar information using the model developed by Wright and Kotey (2006). Once the amount of solar energy absorbed in each layer is determined, the information is passed to the ASHWAT_Thermal module where energy balances are applied to obtain layer temperatures, heat fluxes and indices of merit. The results are then displayed. The solar absorption is shown by arrows proportional to the amount of absorbed solar energy in each layer. The layer temperatures are both overlaid on the system diagram, and written below each layer. The heat flow in each gap is shown numerically, and with arrows to give the sense of the heat flow. Indices of merit are given in a separate window. Figure 4.4, also shown in Appendix A, shows the results screen. Although very few, if any, users will make use of the f_r and C_x values, they are also provided.

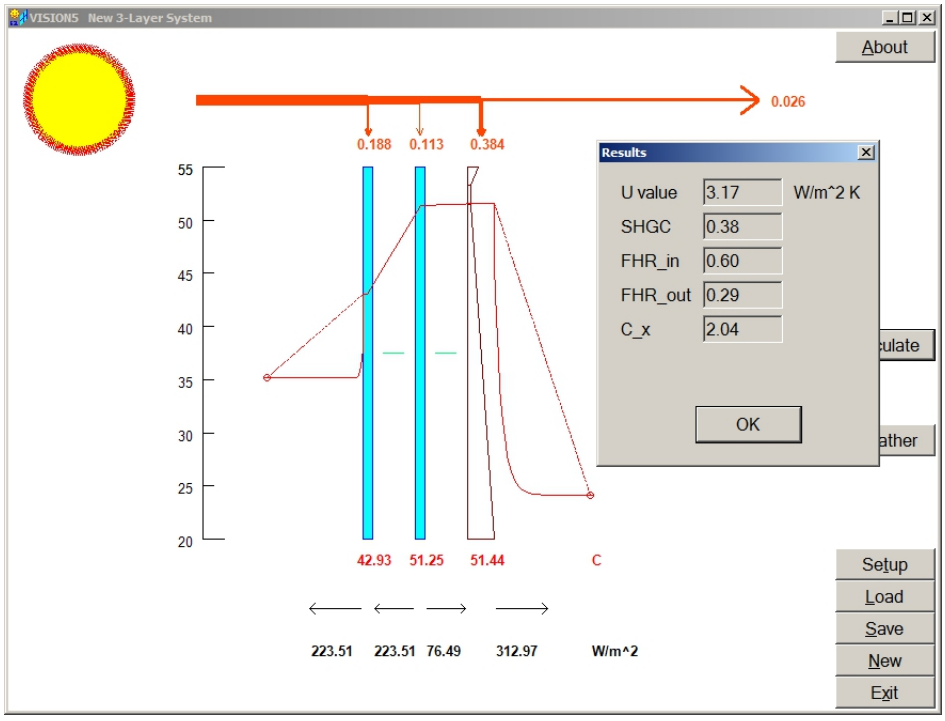

Figure 4.4: Results are both displayed in a pop-up, and overlaid on the system diagram.

4.3 Testing the GUI/DLL Interface

After the correct functioning of the ASHWAT fenestration model was confirmed, the rating tool needed to be tested for accuracy as well. As the calculation engine had already been tested, as described in Chapter 2, the testing was focusing on the user interface and the compatibility between the GUI and the DLL with the calculation programs. This precluded using the test program which had been previously developed, as that program was not compatible with the user-interface. The test cases were manually re-created in the rating tool, and the temperatures, heat fluxes and indices of merit were once again found to agree to four significant digits. As the computational portion of the code is common to both programs, the rating tool was only tested with a few different options to ensure that the different types of layers and gaps could be passed between the user interface and the DLL. The tested cases included various fill gases, multiple shading layers and each type of shading layer and off-normal solar properties for the different layers.

4.4 Sample Fenestration Systems

Figure 4.5 shows a sample fenestration system modelled with the rating tool. The output from the rating tool is shown in Figure 4.5a, and the network which the system was modelled as is shown in Figure 4.5b. This is an unusual configuration, as it contains both a between-panes venetian blind and a pleated drape on the indoor side, in addition to the insect screen on the outdoor side. The temperature of the glazing layer on the outdoor side is lower than the temperature of the adjacent layers. This is possible because this glazing layer has convective heat transfer to the outdoor air, since the gap is vented to the outdoor side, and has radiant exchange with the surroundings which are at $20°C$, rather than the $35°C$ of the ambient air. Additionally, the glazing layer also has radiant exchange with the other glazing layer and the adjacent shading layers, however these will not be contributing to the cooling.

Other systems are shown below to demonstrate the different types of detail that can be modelled by the rating tool. Note that the absorbed fraction of solar flux is shown at the top, rather than the absorbed solar flux. Even in cases where there is no insolation the absorbed fraction is non-zero.

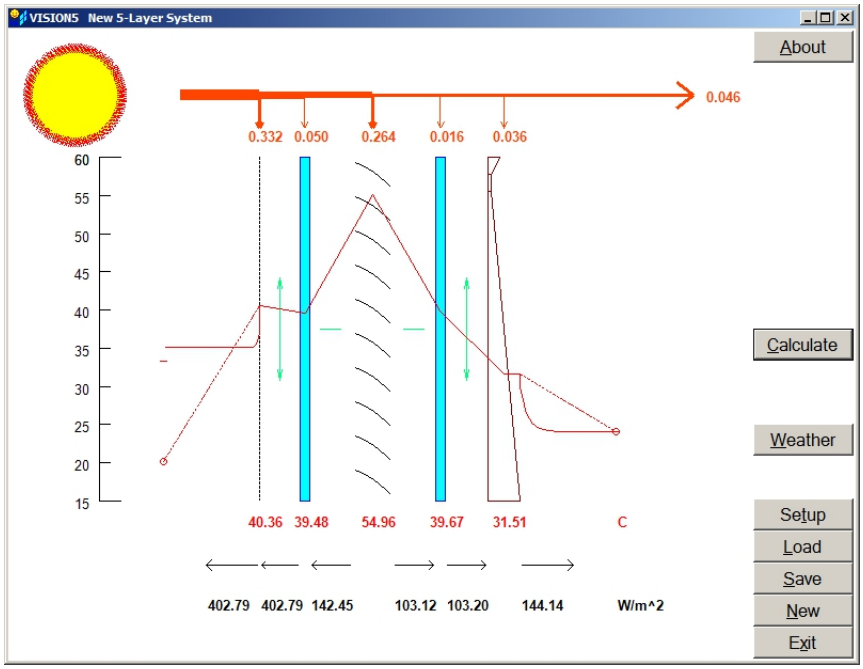

(a) Rating tool output

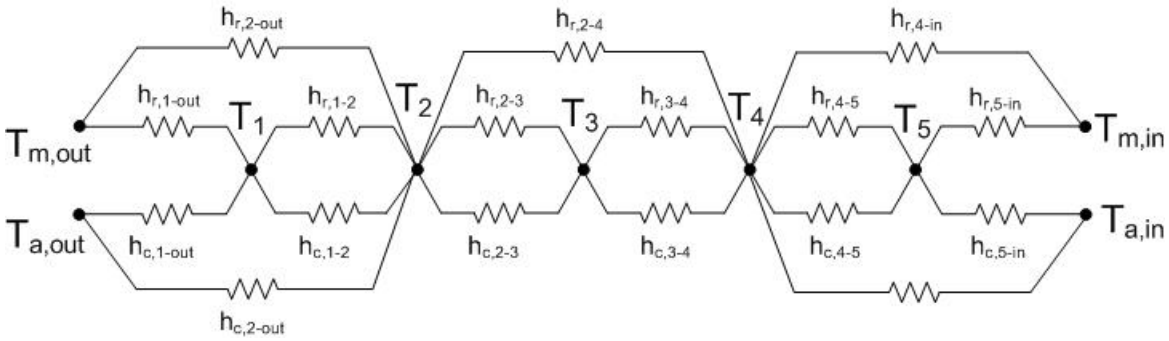

(b) Modelled network

Figure 4.5: A sample 5-layer system. U = 2.89 $\frac{W}{m^2K}$, SHGC = 0.2, $f_{r,in} = 0.39$, $f_{r,out} = 0.12$, $C_x = 2.9\frac{W}{m^2K}$. Notice that the temperature of layer 2 is lower than the temperature of either of the adjacent layers.

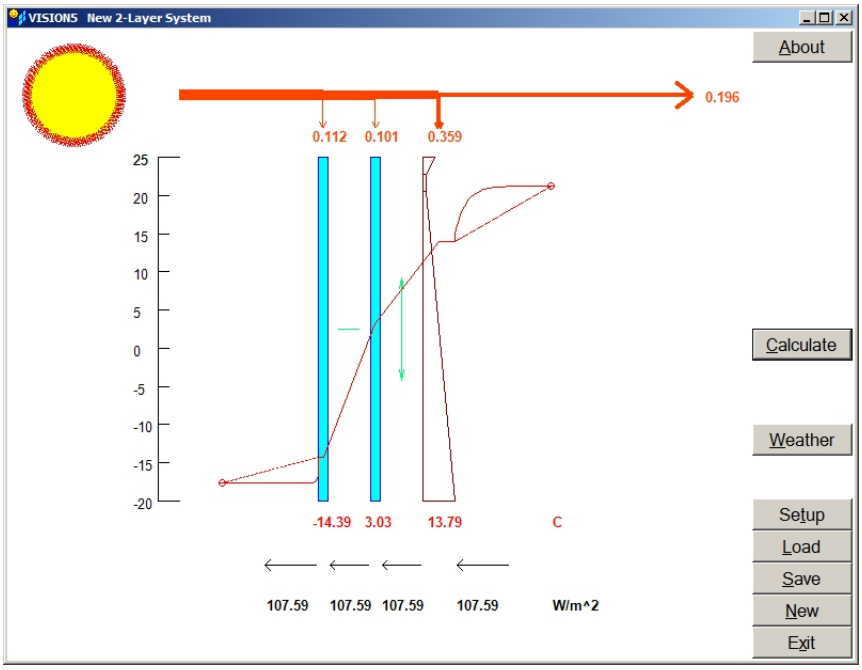

Figure 4.6: A simple double glazed system with a pleated drape on the indoor side tested at the ASHRAE winter condition. U = 2.76 $\frac{W}{m^2K}$, SHGC = 0.55, $f_{r,in} = 0.41$, $f_{r,out} = 0.18$, $C_x = 2.19\frac{W}{m^2K}$.

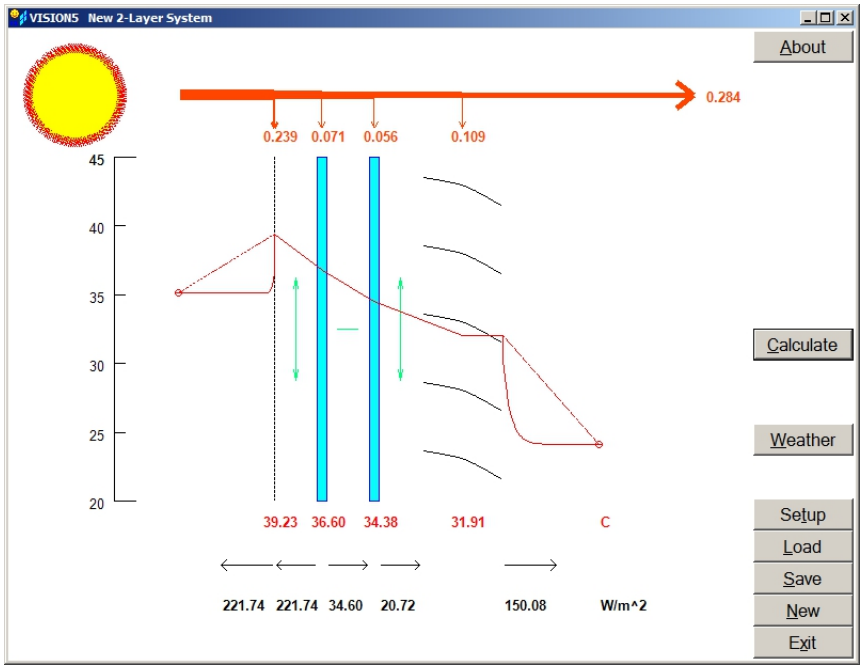

Figure 4.7: A double glazed system with an insect screen on the outdoor side and a venetian blind on the indoor side tested with 20% diffuse radiation and 5% light from the inside. U = 3.79 $\frac{W}{m^2K}$, SHGC = 0.42, $f_{r,in} = 0.39$, $f_{r,out} = 0.17$, $C_x = 2.98\frac{W}{m^2K}$.

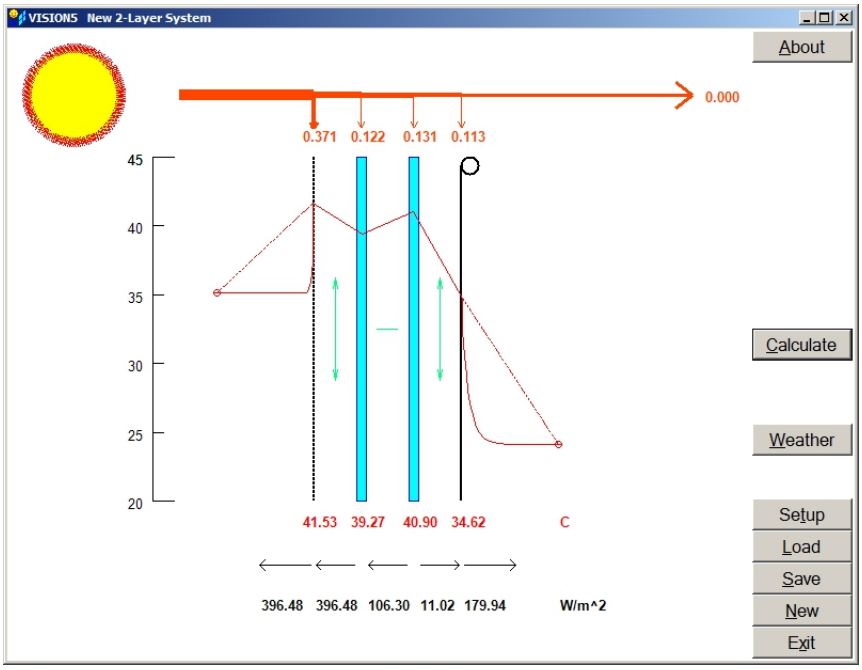

Figure 4.8: A double glazed system with an insect screen on the outdoor side and an opaque roller blind on the indoor side tested with ASHRAE summer condition. U = 3.64 $\frac{W}{m^2K}$, SHGC = 0.18, $f_{r,in} = 0.34$, $f_{r,out} = 0.22$, $C_x = 2.81\frac{W}{m^2K}$.

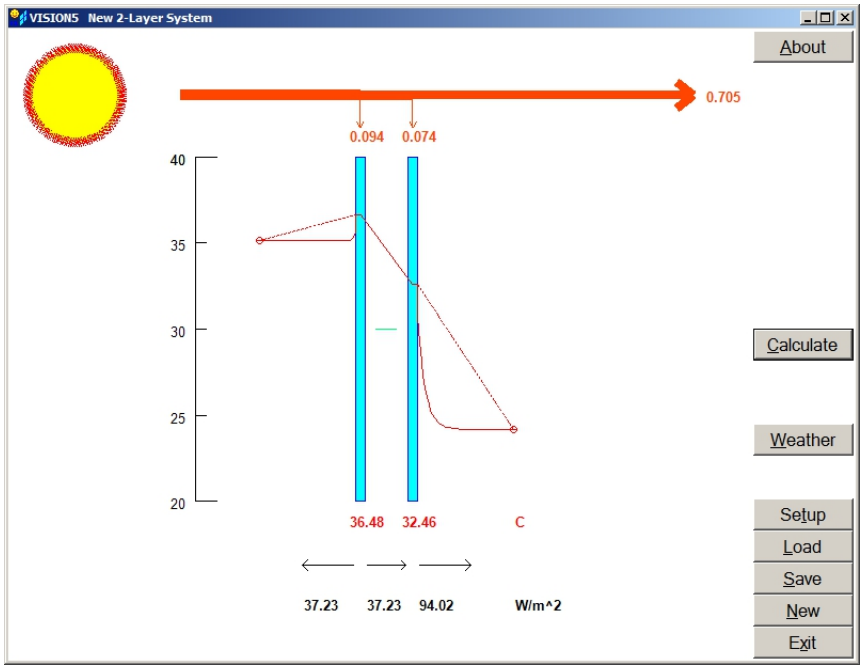

Figure 4.9: A double glazed system tested with ASHRAE summer condition. U = 4.17 $\frac{W}{m^2K}$, SHGC = 0.77, $f_{r,in} = 0.57$, $f_{r,out} = 0.28$, $C_x = 1.65\frac{W}{m^2K}$.

Chapter 5

Conclusions

This project has successfully met its goals, resulting in four noteworthy accomplishments. Three of these are related to the general network theory which is used for the building simulation, and a fourth is more fundamental in nature and relates to measurement techniques which are used to find the properties of shading layers. The network model was integrated into the ASHWAT module; new computational experiments were developed to determine the cross coupling coefficient; a rating tool was developed using the ASHWAT module; and the effects of sample holders projecting into integrating spheres were examined.

The network model has been successfully integrated into the ASHWAT module. The results have been compared against previous implementations and are accurate. A significant improvement in speed was observed in cases with shading devices, and additional speed improvements are available if iteration is disabled or if indices of merit are re-used. Re-using indices of merit has been tested to confirm that the indices of merit are insensitive to changes in the environmental conditions, and found to be reliable. This meets all expectations of the new network model: it is accurate, it is flexible and it requires fewer iterations. This increased speed makes it practical to incorporate the network model into a building simulation program.

New computational experiments were developed to incorporate the network model into the California Simulation Engine. The resulting indices of merit represent the thermal connection between the ambient air and mean radiant temperatures of a conditioned space through the fenestration system. The cross-coupling coefficient can also be found through a computational experiment, allowing the ASHWAT module to be used with building

simulations that use a mean-radiant temperature to characterize the indoor surfaces. The use of the cross-coupling coefficient allows the complex n-resistor network to be simplified to a three-resistor Delta network.

Using the network model, a rating tool was created, from the same calculation engine as was incorporated into the CSE. The rating tool user interface allows people to compare different window types quickly and easily, using multiple shading layers. It allows complex calculations which were not feasible with other window rating tools, due to the flexibility of the solution method and the shading layer models being used. The rating tool gives users complete control over the specified weather conditions: any weather condition can be used, and the rating tool will still provide indices of merit. This makes the rating tool very useful for demonstrating things like the value of shading layers, the value of placing the shading layers on the outdoor side, and of having controllable shading layers, as the effects are isolated from those of the whole building. In addition to allowing the user to see how different fenestration systems handle various weather conditions, the flexibility regarding weather in the calculation engine is what makes integration into the CSE possible. The rating tool fills a niche, and people are glad to have it available for educational and design purposes.

To make off-normal measurements of different shading layer materials, a new measurement technique was developed, using angled sample holders inside of an integrating sphere. Due to the novelty of this technique, more information on the effects of the sample holder were desired. The effects were investigated using a Monte Carlo simulation. The effect of sample holders used to determine the off-normal properties of materials were found to be minor, supporting the models developed using these measurements. The signal strength of the measurement beam was reduced by approximately 20%, although this was corrected for by the dual-beam integrating sphere. In general there was good agreement between the net-radiation analysis and Monte Carlo results. However, both more modelling and more experiments should be done to fully determine the effects of the sample holder tubes, as there were some discrepancies which are still not fully understood.

References

Doe2.com home page. URL http://www.doe2.com/.

Frameplus rating tool. URL http://tools.enermodal.com/webframeplus/WebFRAME_MainPage.aspx.

Powerful connections: Report of the national advisory panel on sustainable energy, science and technology. Technical report, 2006. URL http://www.nrcan.gc.ca/eps/oerd-brde/report-rapport/toc_e.htm.

Charles S Barnaby. correspondence, 2011.

EnergyPlus Engineering Reference. The Board of Trustees of the University of Illinois and the Regents of the University of California through the Ernest Orlando Lawrence Berkeley National Laboratory, October 2010. URL http://apps1.eere.energy.gov/buildings/energyplus/pdfs/engineeringreference.pdf.

Alfred Brunger, Francois M. Dubrous, and Stephen Harrison. Measurement of the Solar Heat Gain Coefficient and U Value of Windows with Insect Screens. *ASHRAE Transactions*, 105(Pt 2):1038–1044, 1999. ISSN 0001-2505.

P.J. Burns, J.D. Maltby, and M.A. Christon. Large-scale surface to surface transport for photons and electrons via monte carlo. *Computing Systems in Engineering*, 1(1): 75 – 99, 1990. ISSN 0956-0521. doi: DOI: 10.1016/0956-0521(90)90049-Q. URL http://www.sciencedirect.com/science/article/B75C5-48TN4J6-5G/2/065ddb61d44572c363db1337dceebfac.

eQuestv3-Overview. California Public Utilities Comission. URL http://www.doe2.com/download/equest/eQUESTv3-Overview.pdf.

John F. Clare. Comparison of four analytic methods for the calculation of irradiance in integrating spheres. *J. Opt. Soc. Am. A*, 15(12):3086–3096, 1998.

M. Collins, J. L. Wright, and N.A. Kotey. Off-normal solar optical property measurements using an integrating sphere. in review, 2010.

DK Edwards. Solar absorption by each element in an absorber-coverglass array. *Solar Energy*, 19:401, 1977. ISSN 0038-092X.

FRAMEplus Online. Enermodal Engineering. URL `http://tools.enermodal.com/webframeplus/`.

David G. Goebel. Generalized Integrating-Sphere Theory. *Applied Optics*, 6(1):125–128, 1967.

Jon W. Hand. *THE ESP-r COOKBOOK Strategies for Deploying Virtual Representations of the Build Environment*. Energy Systems Research Unit of the University of Strathclyde, December 2010. URL `http://www.esru.strath.ac.uk/Documents/ESP-r_cookbook_dec_2010.pdf`.

L. M. Hanssen. Effects of non-lambertian surfaces on integrating sphere measurements. *Appl. Opt.*, 35(19):3597–3606, Jul 1996. URL `http://ao.osa.org/abstract.cfm?URI=ao-35-19-3597`.

L.M. Hanssen. Effects of restricting the detector field of view when using integrating spheres. *Applied optics*, 28(11):2097–2103, 1989.

John A. Jacquez and Hans F. Kuppenheim. Theory of the integrating sphere. *J. Opt. Soc. Am.*, 45(6):460–466, Jun 1955. URL `http://www.opticsinfobase.org/abstract.cfm?URI=josa-45-6-460`.

Kenneth Joong. Master's thesis, University of Waterloo, 2011.

James L. Keef, John F. Clare, and Kurtis J. Thome. Analytical solution for integrating sphere spectral efficiency inclusive of atmospheric attenuation. *Appl. Opt.*, 47(2):253–262, Jan 2008. URL `http://ao.osa.org/abstract.cfm?URI=ao-47-2-253`.

JH Klems. New method for predicting the solar heat gain of complex fenestration systems-I. Overview and derivation of the matrix layer calculation. *ASHRAE Transactions*, 100 (Pt 1):1065–1072, 1994a. ISSN 0001-2505.

JH Klems. New method for predicting the solar heat gain of complex fenestration systems-2. Detailed description of the matrix layer calculation. *ASHRAE Transactions*, 100(Pt 1):1073–1086, 1994b. ISSN 0001-2505.

JH Klems, JL Warner, et al. Solar heat gain coefficient of complex fenestrations with a venetian blind for differing slat tilt angles. *ASHRAE Transactions*, 103(Pt 1):1026–1034, 1997.

N. A. Kotey. *Measurements and models related to solar optics in windows with shading devices*. PhD thesis, University of Waterloo, 2009.

NA Kotey, JL Wright, and MR Collins. Determining off-normal solar optical properties of insect screens. *ASHRAE Transactions*, 115(Pt 1), 2009a.

NA Kotey, JL Wright, and MR Collins. Determining off-normal solar optical properties of roller blind materials. *ASHRAE Transactions*, 115(Pt 1), 2009b.

NA Kotey, JL Wright, and MR Collins. A detailed model to determine the effective solar optical properties of draperies. *ASHRAE Transactions*, 115(Pt 1), 2009c.

NA Kotey, JL Wright, and MR Collins. Determining off-normal solar optical properties of drapery fabrics. *ASHRAE Transactions*, 115(Pt 2), 2009d.

Catalog II 2000-2001. Labsphere Inc., 2000.

A. Laouadi and A. Parekh. Optical models of complex fenestration systems. *Lighting Research and Technology*, 39(2):123, 2007. ISSN 1477–1535.

Bartosz Aleksander Lomanowski. Implementation of window shading models into dynamic whole-building simulation. Master's thesis, University of Waterloo, 2008.

Faye C. McQuiston, P.E. and Jeffrey D. Spitler, P.E. *Cooling and Heating Load Calculation Manual*. American Society of Heating, Refrigerating and Air-Conditioning Engineers, Inc., 2nd edition, 1992.

Robin Mitchell, Christian Kohler, Ling Zhu, and Dariush Arasteh. *THERM 6.3 / WINDOW 6.3 NFRC Simulation Manual*. Lawrence Berkeley National Laboratory, January 2011.

Norman B. Nelson and Barbara B. Prézelin. Calibration of an integrating sphere for determining the absorption coefficient of scattering suspensions. *Appl. Opt.*, 32(33): 6710–6717, Nov 1993. URL `http://ao.osa.org/abstract.cfm?URI=ao-32-33-6710`.

Y. Ohno. Integrating sphere simulation: application to total flux scale realization. *Appl. Opt.*, 33(13):2637–2647, May 1994. URL `http://ao.osa.org/abstract.cfm?URI=ao-33-13-2637`.

G. V. Parmelee and W. W. Aubele. The shading of sunlit glass - an analysis of the effect of uniformly spaced opaque slats. *A.S.H.V.E. Transactions*, 58:377–398, 1952.

GV Parmelee, WW Aubele, and DJ Vild. The Shading of Sunlit Glass: an Experimental Study of Slat-Type Sun Shades. *ASHVE Transactions*, 59:221–240, 1953.

P. Pfrommer, KJ Lomas, and CHR Kupke. Solar radiation transport through slat-type blinds: a new model and its application for thermal simulation of buildings. *Solar Energy*, 57(2):77–91, 1996. ISSN 0038-092X.

Alexander V. Prokhorov, Sergey N. Mekhontsev, and Leonard M. Hanssen. Monte carlo modeling of an integrating sphere reflectometer. *Appl. Opt.*, 42(19):3832–3842, Jul 2003. URL `http://ao.osa.org/abstract.cfm?URI=ao-42-19-3832`.

Robert Siegel and John Howell. *Thermal Radiation Heat Transfer*. Taylor & Francis, New York, NY, 4th edition, 2002.

Herbert L. Tardy. Matrix method for intergrating-sphere calculations. *J. Opt. Soc. Am. A*, 8(9):1411–1418, 1991.

A.H. Taylor. The measurement of diffuse reflection factors and a new absolute reflectometer. *J. Opt. Soc. Am.*, 4:9–23, 1920.

J. Wright and HF Sullivan. Simulation and measurement of windows with low emissivity coating used in conjunction with teflon inner glazings. *International Conference on Building Energy Management, Lausanne, Switzerland*, 4, 1987.

JL Wright. Effective u-values and shading coefficients of preheat/supply-air glazing systems. In *Proc. Solar Energy Society of Canada*, 1986.

J.L. Wright. Calculating center-glass performance indices of windows. *ASHRAE Transactions*, 104(Pt 1):1230–1241, 1998.

J.L. Wright. Calculating center-glass performance indices of glazing systems with shading devices. *ASHRAE Transactions*, 114(Pt 1):471–482, 2008.

J.L. Wright and N.A. Kotey. Solar absorption by each element in a glazing/shading layer array. *ASHRAE Transactions*, 112(Pt 2):3–12, 2006.

J.L. Wright and A. McGowan. Calculating solar heat gain of window frames. *ASHRAE Transactions*, 105(Pt 2):1011–21, 1999.

J.L. Wright, C.S. Barnaby, P. Niles, and C.J. Rogalsky. Efficient simulation of complex fenestration systems in heat balance room models. *12th International Conference of the International Building Performance Simulation Association Sydney Australia, in press*, 2011.

DS Yahoda and JL Wright. Methods for calculating the effective solar-optical properties of a venetian blind layer. *ASHRAE Transactions*, 111(Pt 1):572–586, 2005.

Appendix A

User Guide

Overview

The basic principle behind the user interface is that parts of the complex fenestration system can be examined by right clicking, and changed by left clicking. Information about the system or a given layer is shown in pictorial form: a graphic of the sun is used to represent the outdoor side of the system; arrows are used to show reflectance and transmittance values. There are very few constraints on what can be combined in this system, so you must check that your system carefully.

New System

When you create a new system, you are given the option to set the number of layers, to a maximum of eight (Figure A.1). These layers are all basic glazing layers, and can be changed to other glazing types or shading layers. Layers can be added or removed later. Layers are added through the Edit Gap dialogue, and deleted through the Edit Layer dialogue.

Editing Layers

The Edit Layer dialogue, as it appears when a glazing layer is selected, is shown in Figure A.2. To access it, left-click on any existing layer. The layer number, based on the position of the layer within the complex fenestration system, is shown in the title bar. At the top of the dialogue, the layer number, name and type are displayed. These are not user-editable, and stored in the library for each layer that can be used. This dialogue also gives the option of deleting the selected layer.

The majority of changes which are made to a layer are done by replacing the layer. To replace the layer, select the layer type using the radio buttons, and go to the layer library. In the Library dialogue, shown in Figure A.3, select the library in the left-hand pane and the layer in the right-hand pane.

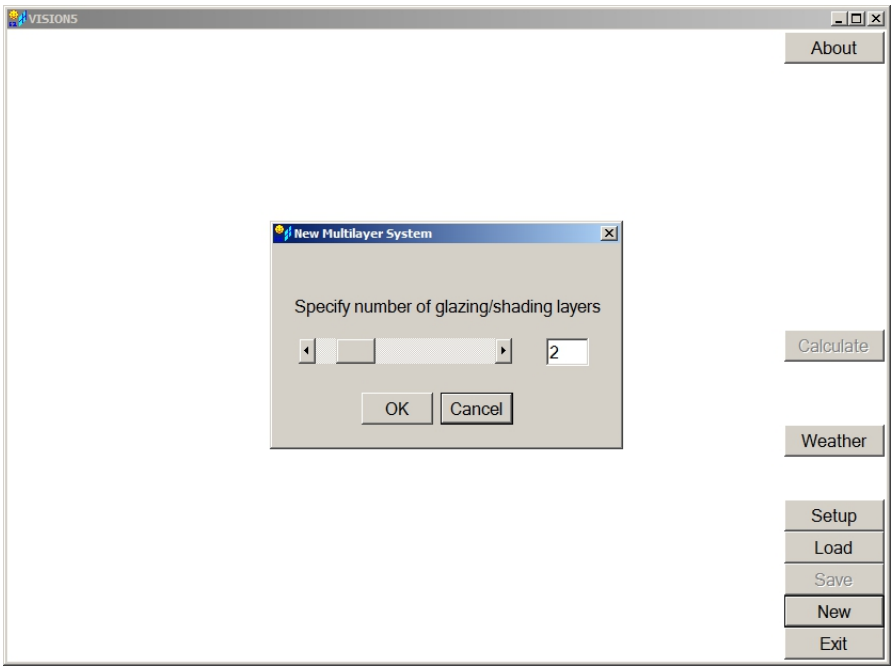

Figure A.1: When creating a new system, you can select the number of layers with which the system is initially constructed.

If the selected layer is a Venetian blind or pleated drape, you will be asked to set additional properties of the layer. For a Venetian blind, the slat angle and whether the slats run horizontally or vertically need to be set. The slat angle is shown on the left-hand panel of the dialogue, Figure A.4a, and appears from the viewpoint of looking down the slats. The slat orientation is shown in the lower right-hand panel of the dialogue box. For a pleated drape, the dialogue, as shown in Figure A.4b, allows the fullness ratio to be adjusted. The diagram is shown looking down along the fabric. The pleat depth is from side to side, and the width of the drape runs from top to bottom.In both cases the illustration changes as the values are changed, to provide visual feedback.

These properties can be set at any time through the Edit Layer dialogue. If there are user-controlled properties, the button in the lower left corner of the dialogue brings up the control for those properties. If the layer is a glazing layer, that button allows the user to flip the glazing layer and reverse the front and back properties.

To check the properties of a layer that is in the system, right-click on the layer, and the Examine Layer dialogue will be shown. This varies with the type of layer. Figure A.5 shows the Examine Layer dialogue for an insect screen layer. The radio buttons allow you to switch which set of properties are displayed. Geometric properties are available only for

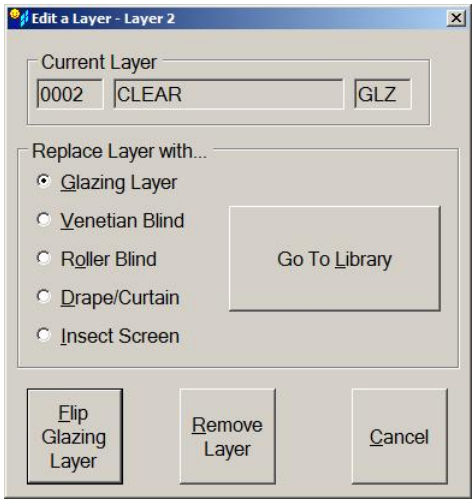

Figure A.2: The Edit Layer dialogue allows you to change or delete the selected layer.

the insect screen and Venetian blind layer types, and do not include slat angle. Properties which do not vary from layer to layer of a given type, such as yarn emissivitiy for roller blinds, are not displayed. Straight arrows represent beam radiation, fan arrows represent diffuse radiation. So beam-diffuse transmission is shown by a single arrow which becomes a fan arrow after it passes through the layer.

Editing Gaps

Just like with layers, you can examine a gap by right-clicking, and edit a gap by left-clicking. Gaps are completely user-controlled. The dialogue for editing gaps, shown in Figure A.6, allows you to adjust the thickness of the gap and to adjust the gap type. Gap types and their meaning are found in Table A.1.If the gap is sealed or stagnant, you can also adjust the gas mixture which fills the gap. To add a sixth gas to the available options, go to the Setup button on the main screen. The Setup dialogue gives the option of adding a user-defined gas. To create a user-defined gas file, set it up following the example (for carbon dioxide) gas file in the GASfiles directory. Each gas needs to have its own file, and should be stored in the GASfiles directory as a .GAS file. Once you loaded a user-defined gas, it will appear in the list of gases available to create the fill gas mixture.

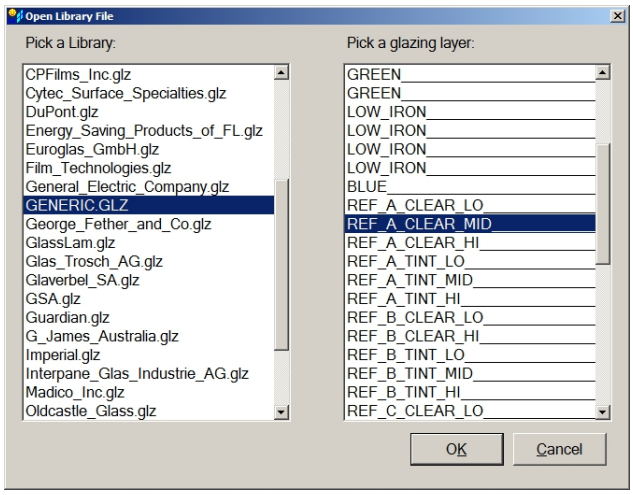

Figure A.3: The Library dialogue allows you to choose a library file and a layer to use

If you save a system that contains a user-defined gas, the user-defined gas is saved with the system information - you do not need to have that gas file available to open the system.

Information about the gaps can be seen by looking at the gap symbols in the system drawing. Figure A.8 shows all the different types of gap symbols. The symbol for a normal gap is drawn solidly if the fill gas is 100% air, and is drawn with a dotted line if the fill gas is not 100% air. To examine the properties of a gap, right-click and the examine gap dialogue, Figure A.7, will be opened. The dialogue shows the gap type, the gap thickness and the fill gas composition. The gas properties of the fill gas mix are shown two ways. The coefficients to describe properties in the form a + bT are given, and the actual values for the properties are shown for a temperature described by the slider bar.

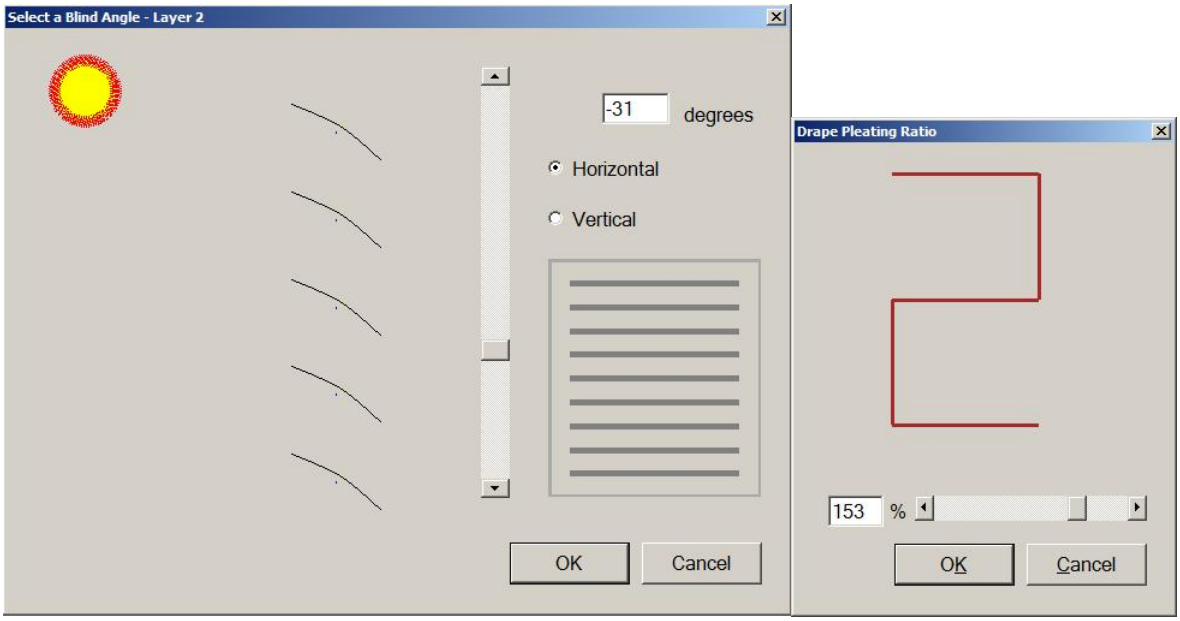

(a) To adjust blind angle and orientation (b) To adjust pleating ratio

Figure A.4: Dialogues for adjusting layer-specific properties of shading layers

Gap Type	Meaning
Normal	Regular sealed gap. Heat transfer is radiation and conduction between layers. Default.
Vented Indoors	Air circulates between the gap and the indoor side of the complex fenestration system. Heat transfer is radiation, convection between the layers, and convection to the indoor side. The fill gas for this gap must be air. This is only an option for the innermost gap.
Vented Outdoors	As Vented Indoors, but to the outdoor, and for the outermost gap.
Stagnant	A sealed gap with no air motion. Heat transfer is through radiation and conduction through the gap.
Evacuated	No fill gas. Heat transfer is through radiation only.

Table A.1: Gap Types

Weather

The weather dialogue, as shown in Figure A.9, allows the user to set the insolation levels, the interior and exterior temperatures and the solar angles. The default method of setting

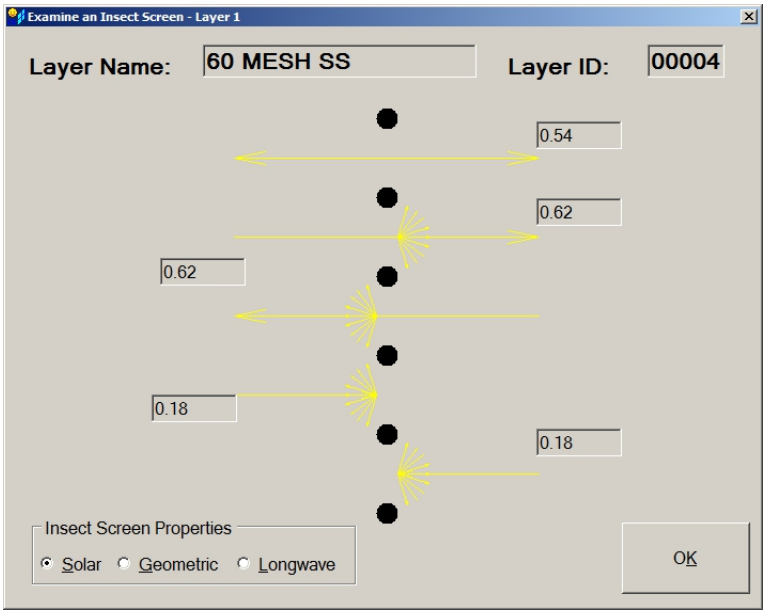

Figure A.5: The Examine Layer dialogue for an insect screen layer. Radio buttons in the lower left corner allow you to switch which properties are shown.

the insolation level is to assign a percentage to each type of insolation - beam, diffuse and indoor (which is assumed to be diffuse). This allows the SHGC to be calculated even if there is no insolation. Alternatively, if you click on the "Calculator" button, a window pops up with fields for filling in numerical values for each type of radiation instead. The solar angle is set using the fields at the bottom of the dialogue. The diagram changes as the angle is adjusted to give visual confirmation of the angle being set.

The temperatures must be set manually, the defaults are 0°C. The mean radiant temperatures are independent of the ambient air temperatures, and both must be manually set. Note that the "h" coefficients are the convective coefficients, not combined. The radiative coefficients are calculated using the layer temperatures and the indoor and outdoor mean radiant temperatures. Alternatively, the ASHRAE winter and summer design conditions can be selected, which will set insolation, temperatures and convective coefficients.

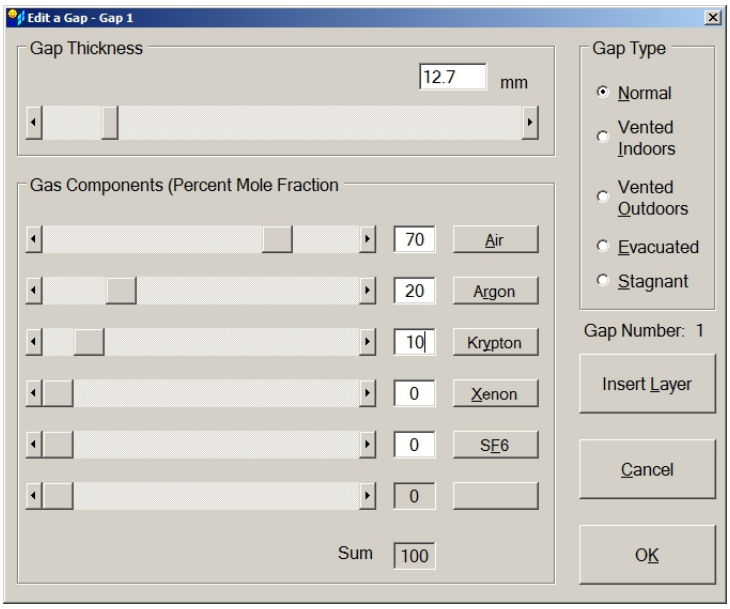

Figure A.6: The dialogue to edit a gap. The gap thickness and type can be altered, as well as the composition of the fill gas

Results

After hitting the Calculate button, you will be prompted to set the weather conditions if you have not already done so. If the weather conditions are set, the results will appear on the screen. Numerical values for indices of merit are given in a pop-up. Provided values are the U-factor, the solar heat gain coefficient, the radiant fraction for both indoor and outdoor heat transfer, and the cross-coupling coefficient. Along the top, the fraction of solar radiation absorbed by each layer and by the room is shown. These numbers are based on the total incoming radiation, not only on the absorbed radiation, and so do not sum to 1. Along the bottom, the total net heat flow in each gap, and from the window to the indoor side and outdoor side is shown. The sense is given by the directions of the arrows, and the magnitude is printed underneath.

Temperature is shown visually by a line overlaid on the system diagram, with a scale on the left. The temperature of each layer, which is assumed to be constant, is printed under the layer. The outdoor and indoor mean radiant temperatures are shown connected to the temperature of the first and last layers by a straight dotted line. The ambient air temperatures are shown by a solid line curving to the temperature. The effective ambient temperature is marked with a line.

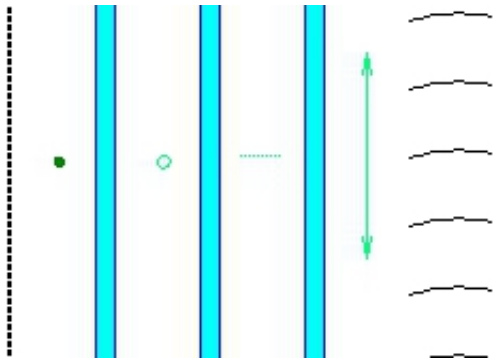

Figure A.7: The different gap symbols. From left to right: stagnant, evacuated, normal (with fill gas other than air) and vented indoors. The symbol for vented outdoors is the same as for vented indoors.

Saving Systems

Created systems can be saved and loaded again later. When you click the Save button, a pop-up will confirm the save format. This is only an issue if the save file will be used in other simulation programs either. The save format can be changed by clicking the Setup button and switching the selected format. Figure A.11 shows the Setup dialogue. The Setup dialogue also gives the option to re-name the system. This name will show in the title bar, and is saved when the system is saved. The pop-up confirming the save format can be turned off. Another option is to load a user-defined gas from a gas library file.

To load a saved system, simply click the Load button, and select the desired system file from the directory in which it was saved. If you intend to use the system in either ESP-r or in the ASHRAE toolkit, make sure that the correct format is selected, by using the Setup dialogue. Weather information is not saved, although if you have included a user-defined gas it is saved in the save file and does not need to be on a computer to open the saved

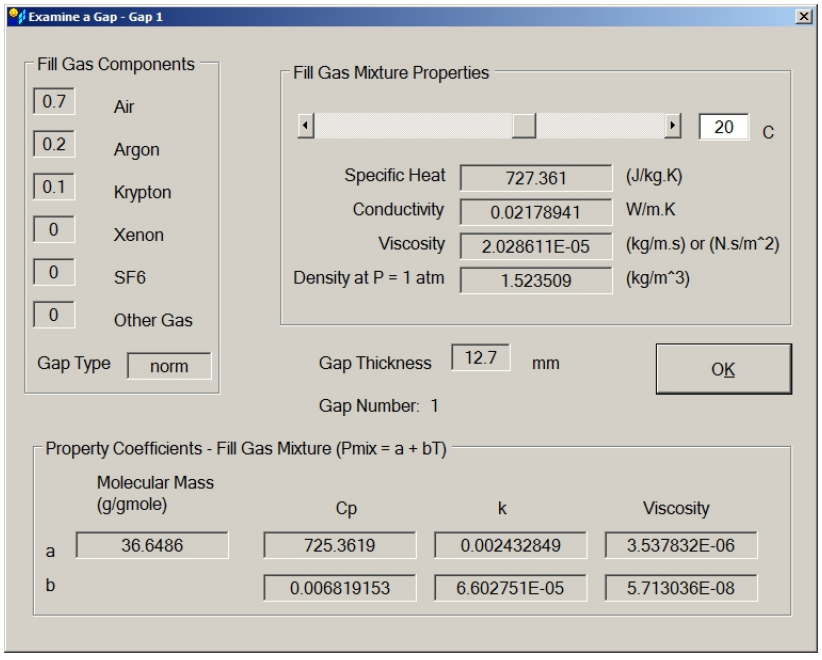

Figure A.8: The dialogue to examine gap properties. Gap thickness, type, and fill gas composition are shown, as well as the gas properties of the fill gas mix.

system.

Layer Properties

Creating new layers

Each layer type has a different format for storing layer information. To be able to create a new layer, create a new library file, and add layers following the layer format guide. The format guides are in files named XXXformat.txt, where XXX is replaced by the three letter layer type abbreviation, as shown in Table A.2. Not all values are stored in the library files for every layer type. If a given value is not shown in the format guide, the information is either assumed, see Defaults section below, or is a composite of other values. For example, some layer types store the beam total transmittance and the beam-beam transmittance. The beam-diffuse transmittance is the difference between those two values. Properties for

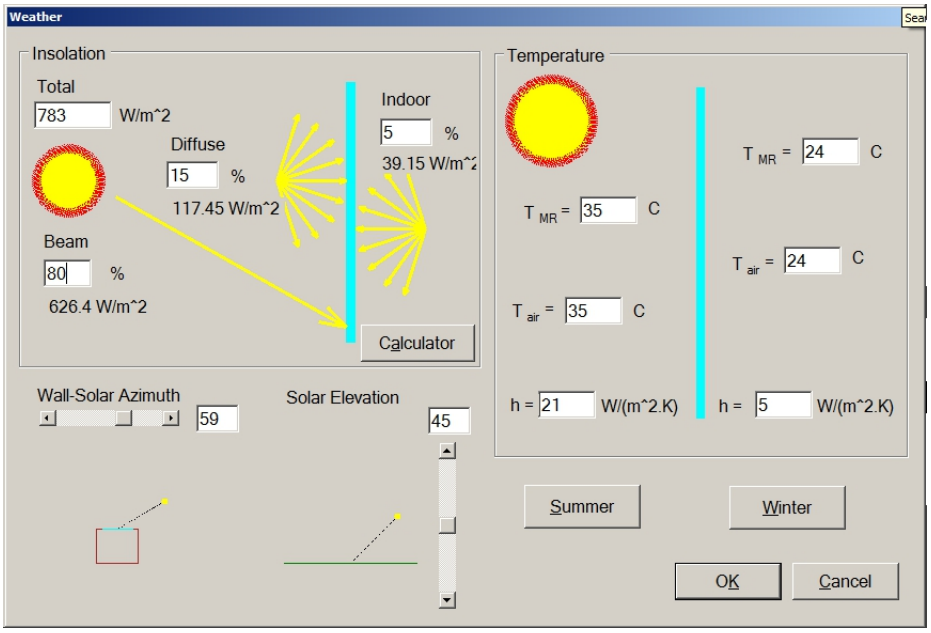

Figure A.9: The Weather dialogue allows you to set the insolation, sun angle, and indoor and temperature and convective coefficients.

incoming diffuse radiation are not stored, as they are calculated from the values for beam radiation.

Layer Type	**Abbreviation**
Glazing Layer	GLZ
Venetian Blind Layer	VBD
Roller Blind Layer	RLD
Pleated Drape Layer	DRP
Insect Screen Layer	BUG

Table A.2: Layer type abbreviations.

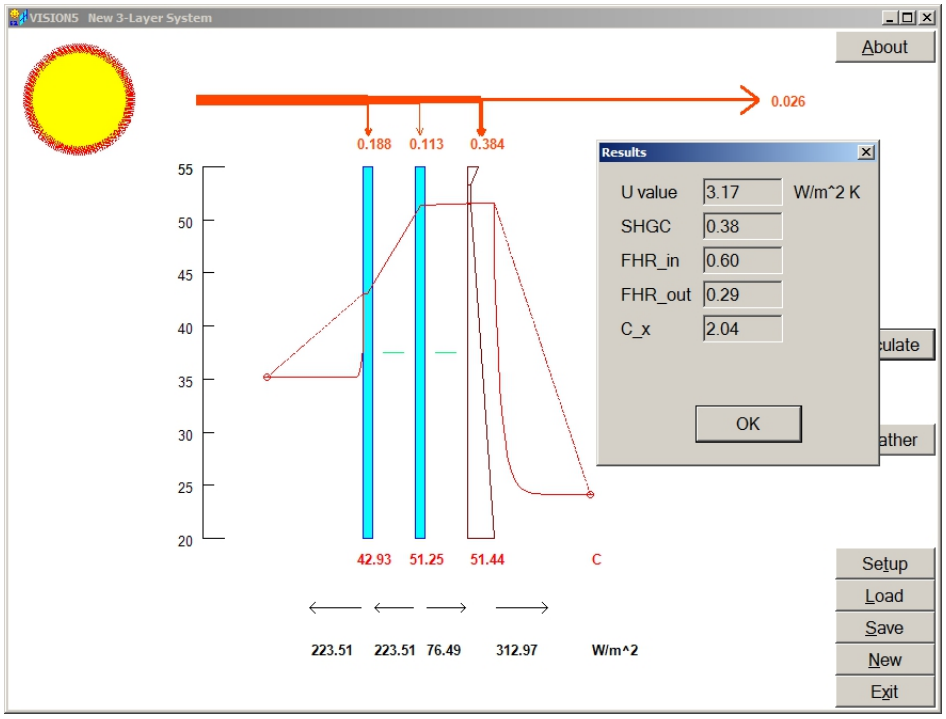

Figure A.10: Results are displayed in a pop-up, and overlaid on the system diagram.

Default Values

Certain default values cannot be changed. Glazing layers are always assumed to be fully specular, so beam-diffuse transmittance and reflectance are always 0. For this reason, beam-beam transmittance is always the same in both directions. Venetian blind slats are assumed to be fully diffuse surfaces, so beam-beam transmittance and reflectivity are 0. Roller blinds, pleated drapes and insect screens are all assumed to have a beam-beam reflectance of 0, although due to geometric considerations the beam-beam transmittance is defined in the libraries. For roller blinds, the layer longwave properties are calculated based on fabric openness, and on assumed yarn emissivity of 0.91 and longwave transmittance of 0.05. Zero-openness fabric for pleated drapes is given an emissivity of 0.87 and a longwave transmittance of 0.05. Wire emissivity for insect screens is defined in the library files, and longwave transmittance is 0.02.

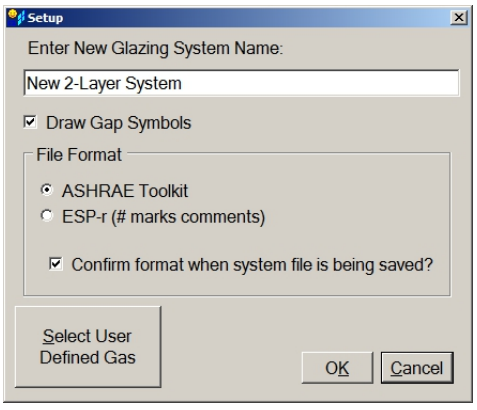

Figure A.11: The Setup dialogue

Appendix B

Convection Heat Transfer Coefficients at Surfaces Exposed to the Environment

Three-Resistor Convection Network

Figure B1 shows the three-resistor network used to model convective heat transfer at surfaces exposed to the environment. The freestream air temperature is T_{air}, the temperature of the shading attachment is T_{shade} and the temperature of the exposed window surface is T_{glass}. It is necessary to evaluate the three heat transfer coefficients associated with the three resistors. More discussion of this network can be found in (Wright 2008), including discussion of jump resistors (e.g., $R_{jump}=(Ah_{g-a})^{-1}$).

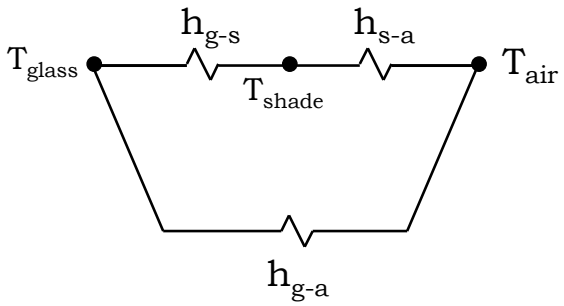

Figure B1: Three-Resistor Network Used to Model Convective Heat Transfer at Surfaces Exposed to the Environment

The two heat transfer coefficients associated with surfaces exposed to the freestream air, h_{s-a} and h_{g-a}, are evaluated by starting with a reference convective heat transfer coefficient, h_c, that is supplied by the user (i.e., the calling routine of the building simulation program). This approach was taken to retain the ability to explore the effect of different boundary conditions such as forced versus natural convection or the differences caused by various styles of air diffusers. The value of h_c can be specified to represent, for example, natural convection ($h_c \approx 3.5 \frac{W}{m^2 K}$) or forced convection ($h_c \approx 20 \frac{W}{m^2 K}$) .

It is also worth noting that each of the resistors shown in Figure B1 exists in parallel with a resistor that applies to radiant heat transfer. For the case of natural convection the radiant mode of heat transfer will be dominant, largely because of the high probability that the emissivity of each component will be high.

Indoor Side

The value of h_{g-s} is estimated by assuming that the airflow between the glass and shade is laminar and for the most part parallel to the glass surface.

$$h_{g-s} = \frac{k_{air}}{b} \qquad \text{(B1)}$$

where k_{air} is the thermal conductivity of air and b is the spacing between the glass and shading layer. When the shading attachment is spaced well away from the window, h_{g-s} will be small and its influence will be unimportant.

Next, the heat transfer coefficients for layer surfaces exposed to the air can be estimated by imposing known limits for extreme values of the spacing, b. When b is large the convective heat transfer at one layer will not be influenced by the presence of the other layer so $h_{g\text{-}a} = h_c$ and $h_{s\text{-}a} = 2\,h_c$. When b approaches zero it can be seen that the shading layer prevents the air from gaining access to the glass, $h_{g\text{-}a} = 0$, and only one side of the shading layer is exposed, $h_{s\text{-}a} = h_c$. A decaying exponential function was used apply a smooth transition between the known limits, with respect to spacing, while noting that the influence of b should disappear as b becomes large. This transition was scaled by assuming that the boundary layers at the glass and shading layer surfaces will not interfere with each other once b exceeds 0.1 m (4 inches). See Equations B2 and B3 as well as Figure B2.

$$h_{g\text{-}a} = h_c\left(1-\exp\left(-4.6\frac{b}{0.1}\right)\right) \qquad \text{b in meters} \qquad \text{(B2)}$$

$$h_{s\text{-}a} = h_c\left(2-\exp\left(-4.6\frac{b}{0.1}\right)\right) \qquad \text{b in meters} \qquad \text{(B3)}$$

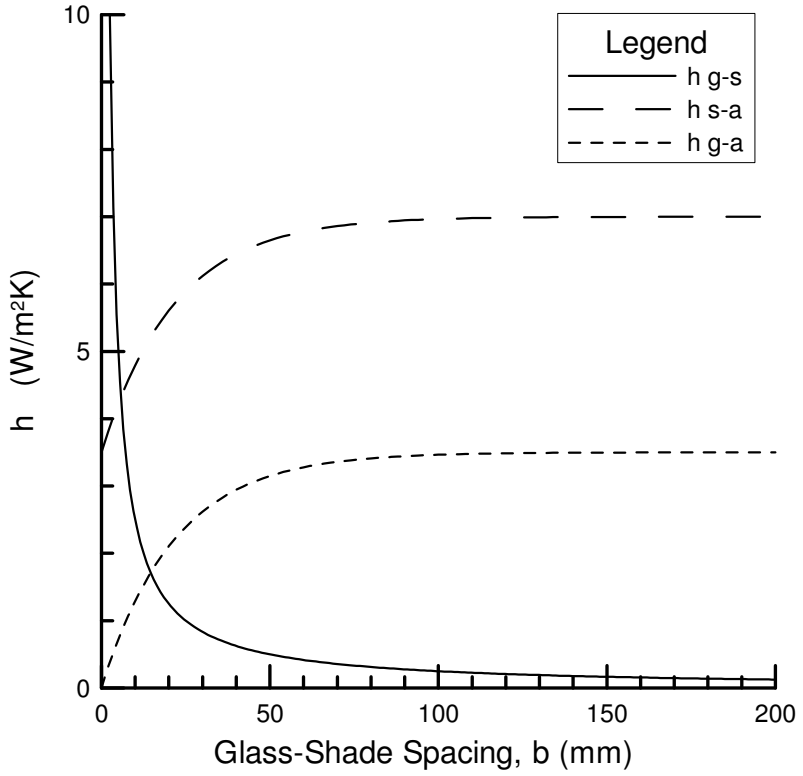

Figure B2: Convective Heat Transfer Coefficients as Functions of Window/Shading Layer Spacing, b, with $h_c \approx 3.5\frac{W}{m^2K}$

One additional adjustment is made for horizontal venetian blinds. It has been noted, on the basis of numerical simulation and interferometry*, that buoyancy will pump an appreciable amount of air through the shading layer when the slats are at any angle other than fully open (slat angle = $\phi = 0$) or fully

closed. Therefore, a factor is calculated as a function of slat angle and applied to augment h_{s-a} by as much as 20%. See Equation B4.

$$h_{s-a} = h_c\left(2 - \exp\left(-4.6\frac{b}{0.1}\right)\right)\cdot\left(1 + 0.2\,|\sin(2\phi)|\right) \qquad \text{b in meters} \qquad \text{(B4)}$$

The maximum value of this factor, 20%, was established by a hand calculation comparing convective heat transfer from a single sloped slat to heat transfer from a large, vertical surface - both in still air .

Note that Equations B1 through B4 are applied in the ASHWAT models by interpreting the gap spacing on the indoor side, b, as an effective gap spacing when a venetian blind is adjacent to the gap. In this case the convective heat transfer coefficients are evaluated as if the venetian blind slats were shortened by 30%. The gap spacing and effective gap spacing are both determined as a function of slat angle and are updated as needed. This model for effective gap spacing (Wright et al. 2008, Huang et al. 2006) was developed for the case of a venetian blind located in a glazing cavity and is applied in the ASHWAT models for venetian blinds attached at the exposed window surface because much of the reasoning related to fill gas or air flow patterns is assumed to apply in both cases. The use of effective gap spacing will have very little influence except for the situation where a venetian blind is placed very close to the glass.

Outdoor Side

Simpler versions of Equations B1 through B3 are applied for unsealed shading layers placed on the outdoor side of the window. In this case, it is likely that h_c will be specified to represent forced convection. Simplifications were used largely because very little is know about the influence of spacing between an outdoor shading attachment and the window. However, it is clear that the presence of convective heat transfer must be accounted for at both surfaces of the shading layer and the exposed surface of the glass. The convection coefficients used on the outdoor side are:

$$h_{g-s} = 0 \qquad \text{(B5)}$$

$$h_{g-a} = h_c \qquad \text{(B2)}$$

$$h_{s-a} = 2\,h_c \qquad \text{(B3)}$$

* Collins, M.R. "Analysis of Solar Heat Gain and Thermal Transmission for Windows with Louvered Shade Systems", Ph.D. Thesis, Queen's University, Kingston, Ontario, 2001